Atmos. Chem. Phys. Discuss., 9, 22041–22101, 2009
www.atmos-chem-phys-discuss.net/9/22041/2009/

Atmospheric Chemistry and Physics Discussions

This discussion paper is/has been under review for the journal *Atmospheric Chemistry and Physics (ACP)*. Please refer to the corresponding final paper in *ACP* if available.

Influences of in-cloud aerosol scavenging parameterizations on aerosol concentrations and wet deposition in ECHAM5-HAM

B. Croft[1], U. Lohmann[2], R. V. Martin[1,3], P. Stier[4], S. Wurzler[5], J. Feichter[6], C. Hoose[7], U. Heikkilä[8], A. van Donkelaar[1], and S. Ferrachat[2]

[1]Department of Physics and Atmospheric Science, Dalhousie University, Halifax, Canada
[2]Institute of Atmospheric and Climate Science, ETH Zurich, Zurich, Switzerland
[3]Harvard-Smithsonian Center for Astrophysics, Cambridge, USA
[4]Atmospheric, Oceanic, and Planetary Physics, University of Oxford, Oxford, UK
[5]Landesamt fur Umwelt, Natur und Verbraucherschutz NRW (LANUV), Recklinghausen, Germany
[6]Max Planck Institute for Meteorology, Hamburg, Germany

[7] Department of Geosciences, University of Oslo, Oslo, Norway
[8] Bjerknes Centre for Climate Research, Bergen, Norway

Received: 23 September 2009 – Accepted: 2 October 2009 – Published: 21 October 2009

Correspondence to: B. Croft (croft@mathstat.dal.ca)

Published by Copernicus Publications on behalf of the European Geosciences Union.

Abstract

A diagnostic nucleation scavenging scheme, which determines stratiform cloud scavenging ratios for both aerosol mass and number distributions, based on cloud droplet, and ice crystal number concentrations, is introduced into the ECHAM5-HAM global climate model. This is coupled with a size-dependent in-cloud impaction scavenging parameterization for both cloud droplet-aerosol, and ice crystal-aerosol collisions. Sensitivity studies are presented, which compare aerosol concentrations, and deposition between a variety of in-cloud scavenging approaches, including prescribed fractions, several diagnostic schemes, and a prognostic aerosol cloud processing treatment that passes aerosol in-droplet and in-ice crystal concentrations between model time steps. For one sensitivity study, assuming 100% of the in-cloud aerosol is scavenged into the cloud droplets and ice crystals, the annual global mean accumulation mode number burden is decreased by 65%, relative to a simulation with prognostic aerosol cloud processing. Diagnosing separate nucleation scavenging ratios for aerosol number and mass distributions, as opposed to equating the aerosol mass scavenging to the number scavenging ratios, reduces the annual global mean sulfate burden by near to 10%. The annual global mean sea salt burden is 30% lower for the diagnostic approach, which does not carry aerosol in-droplet and in-crystal concentrations between model time-steps as compared to the prognostic scheme. Implementation of in-cloud impaction scavenging reduced the annual, global mean black carbon burden by 30% for the prognostic aerosol cloud processing scheme. Better agreement with observations of black carbon profiles from aircraft (changes near to one order of magnitude for mixed phase clouds), ^{210}Pb surface layer concentrations and wet deposition, and the geographic distribution of aerosol optical depth are found for the new diagnostic scavenging as compared to prescribed ratio scavenging scheme of the standard ECHAM5-HAM.

ACPD

9, 22041–22101, 2009

1 Introduction

Atmospheric aerosols significantly influence climate since they both reflect and absorb radiation (direct effects), and modify cloud properties (indirect radiative effects) (Twomey, 1991; Charlson et al., 1992). Aerosols enter cloud droplets, or ice crystals when they act as cloud condensation, or ice nuclei, and also by the process of impaction with the cloud droplets or ice crystals (Pruppacher and Klett, 1997). A fraction of these droplets and crystals will then grow into precipitation particles that are removed from the atmosphere. Global climate models (GCMs) must accurately represent these processes that incorporate aerosols into cloud droplets and ice crystals in order to predict reasonable three-dimensional aerosol distributions, and deposition. Differences in aerosol prediction between global models have been attributed in part to differences in the representation of these removal processes (Textor et al., 2006).

Global models commonly use prescribed fractions to represent the in-cloud scavenging of aerosols, or simply assume that 100% of the aerosol in a cloud is scavenged into the cloud droplets and ice crystals (e.g., Barth et al., 2000; Chin et al., 2000; Takemura et al., 2002; Tie et al., 2005). A lesser number of models use diagnostic in-cloud scavenging schemes, which diagnose the total aerosol scavenged fraction at each model time-step based on selected parameters related to cloud droplet and ice crystal nucleation, such as the supersaturation, updraft speed, and aerosol size and composition (e.g., Adams and Seinfeld, 2002; Gong et al., 2003). Prognostic aerosol cloud processing schemes have also been recently developed, which pass aerosol in-droplet, and in-crystal aerosol concentrations between model time-steps, unlike diagnostic schemes (e.g., Ghan and Easter, 2006; Hoose et al., 2008a,b).

The standard ECHAM5-HAM model represents five aerosol species using a superposition of seven log-normal modes, and in-cloud scavenging ratios are prescribed as a function of aerosol mode, and cloud temperature and type (Stier et al., 2005). In this study, we introduce a new diagnostic in-cloud nucleation scavenging parameterization that is coupled with a size-dependent in-cloud impaction scavenging scheme,

ACPD
9, 22041–22101, 2009

for warm, mixed, and ice phase clouds. By the term diagnostic, we mean that the total aerosol fraction scavenged into the cloud droplets and ice crystals is diagnosed at each model time-step, and unlike in a prognostic scavenging scheme, aerosol in-droplet and in-crystal concentrations are not passed between model time-steps. For our parameterization, the aerosol mass and number distributions are scavenged by separate nucleation scavenging ratios. Ghan and Easter (2006) showed that a diagnostic scheme under-predicted global mean aerosol number burdens by 20% as compared to a prognostic representation of the in-droplet aerosols. However, that study did not explore the bias of using prescribed scavenging fractions, and did not examine sensitivities related to the scavenging of aerosols by ice crystals. Using the ECHAM5-HAM model, this study compares three fundamental in-cloud scavenging approaches, prescribed fractions, diagnostic in-cloud scavenging dependent on the number of cloud droplets and ice crystals, and the prognostic treatment of in-droplet and in-crystal aerosols.

The representation of in-cloud impaction scavenging varies considerably between global models. Many models do not treat this process explicitly, but include the process implicitly in the prescribed scavenging ratios. Gong et al. (2003) used a parameterized equation as a function of the mean cloud droplet and aerosol radii, and cloud droplet number concentration. Hoose et al. (2008a,b) used prescribed collection kernels for each aerosol mode of ECHAM5-HAM. Recently, Baumgardner et al. (2008) have suggested that for black carbon, scavenging by ice crystals is dominated by impaction as opposed to nucleation processes. In this study, we compare the prescribed kernel approach of Hoose et al. (2008a,b) with a physically detailed size-dependent cloud droplet-aerosol, and ice crystal-aerosol impaction scavenging parameterization. Our parameterization selects mean mass and number impaction scavenging coefficients from a look-up table as a function of mean cloud droplet radius assuming a gamma distribution, median radius of the lognormal aerosol mass or number distribution, and cloud droplet number concentration. This is coupled with an ice-crystal-aerosol in-cloud impaction scavenging parameterization that depends on the monodisperse ice crystal radius, ice crystal number concentration, and the median aerosol radius of the

ACPD
9, 22041–22101, 2009

mass and number distributions. The global contribution of impaction scavenging to total deposition is quantified for the five aerosol species: sulfate, black carbon, particulate organic matter, sea salt and dust.

The next section gives a description of the ECHAM5 GCM, coupled to the aerosol scheme HAM, and includes the details of the various in-cloud scavenging parameterizations. Section 3 summarizes the impacts of the in-cloud scavenging parameterizations on the global aerosol three-dimensional distributions and removal rates. Section 4 presents a comparison with observations of aerosol wet deposition, vertical profiles of black carbon concentrations, marine boundary layer size distributions, and aerosol optical depth. This also includes a sub-section on the global modeling of ^{7}Be and ^{210}Pb, which are useful as passive tracers to examine in-cloud scavenging parameterizations. Section 5 gives a summary and conclusions.

2 Model description

ECHAM5 is the fifth generation atmospheric general circulation model (GCM) developed at the Max-Planck Institute for Meteorology (Roeckner et al., 2003), and evolved from the model of the European Centre for Medium Range Weather Forecasting (ECMWF). The model solves prognostic equations for vorticity, divergence, temperature and surface pressure using spheric harmonics with triangular truncation. Water vapor, cloud liquid and ice water are transported using a semi-Lagrangian scheme (Lin and Rood, 1996). Additionally, for this study we have implemented the prognostic equations for cloud liquid and ice water, mass and number following Lohmann et al. (2007), and the cirrus scheme of Lohmann and Kärcher (2002). Convective clouds, and transport are based on the mass-flux scheme of Tiedtke (1989) with modifications following Nordeng (1994). The solar radiation scheme has 6 spectral bands (Cagnazzo et al., 2007) and the infrared has 16 spectral bands (Mlawer et al., 1997; Morcrette et al., 1998). The GCM is coupled to the Hamburg Aerosol Model (HAM), which is described in detail in Stier et al. (2005). The aerosols are represented by seven log-

ACPD
9, 22041–22101, 2009

normal modes, 4 internally mixed/soluble modes (nucleation (NS), Aitken (KS), accumulation (AS), and coarse (CS)), and 3 insoluble modes (Aitken (KI), accumulation (AI),and coarse (CI)). The count median radius for each mode is calculated from the aerosol mass and number concentrations of each mode, which are allowed to vary independently, and with a fixed standard deviation for each mode. Aerosol mass and number are transferred between the modes by the processes of sulfuric acid condensation, and also coagulation between aerosols. All results presented in this study are from a one year simulation, following a three months spin-up period, except 6 months spin-up period for simulations with ^{210}Pb and ^{7}Be. All simulations are nudged towards the meteorological conditions of the year 2001. The nudging approach, combined with aerosol-radiation de-coupling, was chosen in order to have the same dust and sea salt emissions in all simulations. We chose the year 2001 since that was a neutral year for the El Nino Southern Oscillation. The natural emissions of sea salt, dust, and DMS from the oceans are calculated on-line, based on the meteorology of the model. Emissions for all other aerosol species are taken from the AEROCOM emission inventory, and are representative for the year 2000 (Dentener et al., 2006b). The aerosol emissions and the removal processes of sedimentation, and dry deposition are described in detail in Stier et al. (2005). Additionally, the below-cloud scavenging parameterization of Croft et al. (2009) has been implemented for this study.

2.1 In-cloud aerosol scavenging parameterizations

2.1.1 Current in-cloud scavenging

In the standard ECHAM5-HAM model, in-cloud scavenging ratios are prescribed for each of the seven log-normal modes. These ratios depend on the cloud temperature, distinguishing between warm, mixed and ice clouds, and also depend on the cloud type, either stratiform or convective. The cloud scavenging ratios are presented in Table 1. The control (CTL) simulation is conducted with these prescribed ratios of the

standard ECHAM5-HAM model. The rate of change of tracer i is

$$\frac{\Delta C_i}{\Delta t} = R_i C_i f^{\mathrm{cl}} \left(\frac{f^{\mathrm{liq}} Q^{\mathrm{liq}}}{C_{\mathrm{liq}}} + \frac{f^{\mathrm{ice}} Q^{\mathrm{ice}}}{C_{\mathrm{ice}}} \right) \quad (1)$$

where R_i is the prescribed in-cloud scavenging ratio, C_i is the mixing ratio of tracer i, f^{cl} is the cloud fraction, C_{liq} and C_{ice} are the cloud liquid and ice water mixing ratios, respectively, Q^{liq} and Q^{ice} are the respective sums of the conversion rates of cloud liquid and ice to precipitation by the processes of autoconversion, accretion and aggregation, and f^{liq} and f^{ice} are the respective liquid and ice fraction of the cloud water, and Δt is the time-step. Each prescribed in-cloud scavenging ratio combines both nucleation and impaction scavenging in the current model.

2.1.2 New diagnostic in-cloud nucleation scavenging

For the new nucleation scavenging parameterization, the scavenging ratios for stratiform clouds are diagnosed from the cloud droplet number concentration (CDNC), and the ice crystal number concentration (ICNC). The convective in-cloud scavenging for all simulations uses the prescribed ratios given in Table 1, and described in detail in Stier et al. (2005). For stratiform clouds, both the CDNC and ICNC are prognostic variables in the used version of the ECHAM5-HAM model, and the cloud microphysics is described in detail in Lohmann et al. (2007). In our model version, and for all simulations presented in this study, the activation of aerosol particles to form cloud droplets is parameterized using the Ghan et al. (1993) scheme. The number of activated aerosols $N_{\mathrm{act,Ghan}}$ is given by

$$N_{\mathrm{act,Ghan}} = \frac{\omega N_{>35\,\mathrm{nm}}}{\omega + \beta N_{>35\,\mathrm{nm}}} \quad (2)$$

and

$$\omega = \bar{\omega} + 0.7\sqrt{\mathrm{TKE}}\,. \quad (3)$$

ω is the updraft velocity, $\bar{\omega}$ is the large-scale vertical velocity, TKE is the turbulent kinetic energy, β is 0.0034 $cm^4\ s^{-1}$, and $N_{>35\,nm}$ is the total number of soluble/internally mixed aerosols with radius >35 nm.

For the new diagnostic nucleation scavenging scheme the total number of aerosols to be scavenged into the cloud droplets and ice crystals at each time-step is the sum of the CDNC and ICNC. This total must apportioned between each of the four soluble/internally mixed modes. For clouds with temperatures >238.15 K, the apportioning is done following,

$$N_{j,\mathrm{scav}} = (\mathrm{CDNC} + \mathrm{ICNC}) \cdot \frac{N_{j>35\,nm}}{N_{>35\,nm}} \tag{4}$$

where $N_{j,\mathrm{scav}}$ is the total number of aerosols to be scavenged from the jth mode, for j=NS, KS, AS, CS. $N_{j>35\,nm}$ is the aerosol number for the jth mode having radius greater than 35 nm, and $N_{>35\,nm}$ is the number of aerosols having radius greater than 35 nm summed over all the soluble/internally mixed modes. Thus, if tracer i is a soluble/internally mixed number mixing ratio, we have the following nucleation scavenging fraction,

$$R_{i,\mathrm{nuc}} = \frac{N_{j,\mathrm{scav}}}{N_j}. \tag{5}$$

where N_j is the total number of aerosols in the jth mode. The insoluble modes are assumed to have nucleation scavenging ratios of zero, but the impaction scavenging ratio might not be zero.

For this diagnostic scavenging scheme, for any given aerosol mode, the scavenged fraction of the mass distribution is not set equal to the scavenged fraction of the number distribution. To determine the fractional scavenging of the mass distribution, the aerosols in each mode are assumed to be scavenged progressively from the largest to the smallest size. Thus, for each mode a critical radius, $r_{j,\mathrm{crit}}$, can be determined that has exactly $N_{j,\mathrm{scav}}$ in the lognormal tail of the number distribution. The total aerosol

ACPD
9, 22041–22101, 2009

mass to be scavenged from the jth mode is that mass of the lognormal tail that lies above $r_{j,\mathrm{crit}}$.

To calculate $r_{j,\mathrm{crit}}$, the cumulative log-normal size distribution, $F_N(r_{j,\mathrm{crit}})$, is employed, where

$$F_N(r_{j,\mathrm{crit}}) = N_j - N_{j,\mathrm{scav}} = \frac{N_j}{2} + \frac{N_j}{2}\mathrm{erf}\left(\frac{\ln(r_{j,\mathrm{crit}}/r_{\mathrm{pg}})}{\sqrt{2}\ln\sigma_g}\right) \quad (6)$$

and r_{pg} is the count median radius for the jth mode, σ_g is the standard deviation for the respective mode and erf refers to the error function. By taking a rational approximation to the inversion of the error function, the above equation can be solved for $r_{j,\mathrm{crit}}$. Thus, the critical radius is given by,

$$r_{j,\mathrm{crit}} = r_{\mathrm{pg}} \cdot \left(\exp\left(\sqrt{2}\ln\sigma_g \cdot \mathrm{erf}^{-1}\left(1 - \left(2 \cdot (\mathrm{CDNC} + \mathrm{ICNC}) \cdot \frac{N_{j>35\,\mathrm{nm}}}{N_j N_{>35\,\mathrm{nm}}}\right)\right)\right)\right) \quad (7)$$

where $N_{j,\mathrm{scav}}$ has been replaced the explicit expression in Eq.(4). Therefore, if tracer i is a soluble/internally mixed mass mixing ratio we have the following nucleation scavenging fraction for the mass distribution,

$$R_{i,\mathrm{nuc}} = \frac{\int_{r_{j,\mathrm{crit}}}^{\infty} m_{i,j}(r_{\mathrm{p}})dr_{\mathrm{p}}}{\int_0^{\infty} m_{i,j}(r_{\mathrm{p}})dr_{\mathrm{p}}} \quad (8)$$

where $m_{i,j}(r_{\mathrm{p}})$ is the lognormal mass distribution for the ith aerosol species of the jth mode, and r_{p} is the aerosol radius. The lognormal mass distribution has the same standard deviation as the number distribution for any given mode, as described in Stier et al. (2005), and the mass median radius for the lognormal distribution ($r_{\mathrm{pg,m}}$) is related to the count median radius (r_{pg}) following

$$r_{\mathrm{pg,m}} = r_{\mathrm{pg}} \cdot \exp(3\ln^2\sigma_g). \quad (9)$$

The nucleation scavenging for temperatures below 238.15 K is slightly different, since homogeneous freezing can occur at these temperatures. The used version of the ECHAM5-HAM includes a cirrus scheme as described in Lohmann and Kärcher (2002). The total ICNC is assumed to be equal to the total number of aerosols to be scavenged, but the modes are scavenged progressively from the largest soluble/internally mixed mode (CS) to the smallest (KS). As a result, the calculation of the critical radius, is only done for the mode that is found to be partially scavenged, after all larger modes are fully scavenged. The nucleation scavenging ratio is set to zero for all modes smaller than the partially scavenged mode, and for all insoluble modes.

2.1.3 New size-dependent in-cloud impaction scavenging

For the aerosol-cloud droplet impaction scavenging, the mean mass scavenging coefficients, in units of inverse time, are

$$\Lambda_{\mathrm{m}}(r_{\mathrm{pg,m}}) = \frac{\int_0^\infty \Lambda(r_{\mathrm{pg,m}}) r_{\mathrm{p}}^3 n(r_{\mathrm{p}}) dr_{\mathrm{p}}}{\int_0^\infty r_{\mathrm{p}}^3 n(r_{\mathrm{p}}) dr_{\mathrm{p}}}, \tag{10}$$

and the mean number scavenging coefficients are

$$\Lambda_{\mathrm{n}}(r_{\mathrm{pg}}) = \frac{\int_0^\infty \Lambda(r_{\mathrm{pg}}) n(r_{\mathrm{p}}) dr_{\mathrm{p}}}{\int_0^\infty n(r_{\mathrm{p}}) dr_{\mathrm{p}}}, \tag{11}$$

where $n(r_{\mathrm{p}})$ is the aerosol lognormal number distribution, r_{p} is the aerosol radius, and r_{pg}, and $r_{\mathrm{pg,m}}$ are the median aerosol radius for the number and mass distribution, respectively. The scavenging coefficient $\Lambda(r_{\mathrm{pg}})$, also in units of inverse time, is defined as

$$\Lambda(r_{\mathrm{pg}}) = \int_0^\infty \pi R_{\mathrm{liq}}^2 U_{\mathrm{t}}(R_{\mathrm{liq}}) E(R_{\mathrm{liq}}, r_{\mathrm{pg}}) n(R_{\mathrm{liq}}) dR_{\mathrm{liq}} \tag{12}$$

where R_{liq} is the cloud droplet radii, $U_{\mathrm{t}}(R_{\mathrm{liq}})$ is the terminal velocity of the cloud droplet, $E(R_{\mathrm{liq}}, r_{\mathrm{p}})$ is the collision efficiency between the aerosol and cloud droplet, and $n(R_{\mathrm{liq}})$

is the cloud droplet number distribution, which is assumed to be a Gamma distribution. We find the collision efficiencies and terminal velocities following the approach outlined in detail in Croft et al. (2009). Figure 1 shows the impaction scavenging coefficients for a CDNC of 40 cm^{-3} as an example. The scavenging coefficients have a minimum for aerosol radii near to 0.1 μm. For aerosols with radii smaller than 0.1 μm, Brownian motion increases their collection by the cloud droplets, whereas the inertia of larger aerosols increases their collection. At the minima, neither of these forces is dominant. The impaction scavenging coefficients are compiled in look-up tables. Thus, if tracer i is a mass mixing ratio, the scavenging fraction for cloud droplet-aerosol impaction is

$$R_{i,\mathrm{imp,liq}} = \Lambda_{\mathrm{m}}(r_{\mathrm{pg,m}})\Delta t \tag{13}$$

and likewise if tracer i is a number mixing ratio, but using $\Lambda_{\mathrm{n}}(r_{\mathrm{pg}})$. Both soluble/internally mixed, and insoluble aerosol modes are scavenged similarly by impaction.

Since the ECHAM5-HAM model assumes that the ice crystals are monodiperse, we do not integrate over an ice crystal number distribution to determine the scavenging ratio, but rather the scavenged fraction due to aerosol-ice crystal impaction is defined as

$$R_{i,\mathrm{imp,ice}} = K(R_{\mathrm{ice}}, r_{\mathrm{pg}}) \cdot \mathrm{ICNC} \cdot \Delta t \tag{14}$$

where ICNC is the ice crystal number concentration, and R_{ice} is the radius of the maximum dimension of the ice crystal, and r_{pg} is the median radius of the aerosol number, or mass distribution, and $K(R_{\mathrm{ice}}, r_{\mathrm{p}})$ is the collection kernel given by,

$$K(R_{\mathrm{ice}}, r_{\mathrm{pg}}) = \pi R_{\mathrm{ice}}^2 U_{\mathrm{t}}(R_{\mathrm{ice}}) E(R_{\mathrm{ice}}, r_{\mathrm{pg}}) \tag{15}$$

The collection kernels are taken from Miller and Wang (1991) in units of $cm^3\,s^{-1}$ and are compiled in look-up tables in our model. For temperatures less than 238.15 K, we assume that all crystals are columns, and for temperatures greater than 238.15 K, all crystals are assumed to be plates (Lohmann et al., 2008). There is a lack of collection

data for ice crystals with radii less than about 30 μm. For these crystal sizes, we use the same collection kernels as for liquid droplets, as described in detail in Croft et al. (2009). Ice crystals of this size are often assumed to be quasi-spherical (Spichtinger and Gierens, 2009). Figure 2 shows the collection kernels for ice plates and columns for a selection of Reynold's numbers, and also for droplets with radii of 30 μm and less. In our look-up table approach, the Reynold's number is related to the size of the ice crystals following the crystal dimensions given in Martin et al. (1980), and Miller and Wang (1989). Similar to droplets, ice crystals have a scavenging minimum, but this minimum shifts due to the various geometries of the crystals. For particle sizes near the scavenging minimum, plates are more efficient scavengers than columns. Miller and Wang (1991) attribute this to the formation of eddies in the flow around the plate geometry, which increases their collection. Similar to Eq. (1), the local rate of change of the tracer C_i due to in-cloud scavenging by both nucleation and impaction is

$$\frac{\Delta C_i}{\Delta t} = C_i f^{\mathrm{cl}} \left(\frac{(R_{i,\mathrm{nuc}} + R_{i,\mathrm{imp,liq}}) f^{\mathrm{liq}} Q^{\mathrm{liq}}}{C_{\mathrm{liq}}} + \frac{(R_{i,\mathrm{nuc}} + R_{i,\mathrm{imp,ice}}) f^{\mathrm{ice}} Q^{\mathrm{ice}}}{C_{\mathrm{ice}}} \right) \tag{16}$$

where f^{liq} and f^{ice} are the respective liquid and ice water fractions of the total cloud water, f^{cl} is the cloud fraction, C_{liq} and C_{ice} are the cloud liquid and ice water content, respectively, and Q^{liq} and Q^{ice} are the respective sums of the conversion rates of cloud liquid and ice to precipitation by the processes of autoconversion, accretion and aggregation. This diagnostic scavenging approach is implemented in simulation DIAG-FULL.

2.1.4 Prognostic in-cloud scavenging

In this study, we also use the prognostic in-cloud aerosol processing scheme for stratiform clouds developed by Hoose et al. (2008a,b) (simulation PROG-AP). This scheme treats the aerosol mass and number concentrations in the cloud droplets and ice crystals as prognostic species, which are passed between model time-steps. The

ACPD
9, 22041–22101, 2009

methodology is described in detail in Hoose et al. (2008a,b). Unlike the new diagnostic scheme, the prognostic scheme applies the same scavenging ratio to both the aerosol mass and number distributions for any given aerosol mode, grid box and time-step, as opposed to having separate mass and number scavenging ratios. One other difference is that the in-cloud impaction scavenging implements the prescribed kernels of Table 2 as opposed to the physically detailed size-dependent impaction parameterization of the new diagnostic scheme in the simulation DIAG-FULL.

2.1.5 Diagnostic in-cloud scavenging sensitivity simulations

We implement several variations to the new diagnostic scheme as sensitivity tests. Simulation DIAG2 replaces the size-dependent in-cloud impaction parameterization of simulation DIAG-FULL with the prescribed impaction kernels of Hoose et al. (2008a,b) given in Table 2. DIAG2 is otherwise the same as DIAG-FULL. Simulation DIAG1 differs from simulation DIAG2 only in that the mass nucleation scavenging ratios are set equal to the number nucleation scavenging ratios. Otherwise DIAG2 and DIAG1 are the same. Two additional sensitivity studies are done to examine the prescribed ratio approach. 100% of the aerosols in clouds are assumed to be scavenged into the droplets or crystals for the simulation F100. This simplistic assumption has been used in global models (e.g., Barth et al., 2000). The simulation F100-INT is similar except that 100% of the soluble/internally mixed aerosols in clouds are assumed to be cloud-borne, and 0% of the insoluble aerosol is scavenged into the cloud droplets or crystals. All simulations are summarized in Table 3.

3 Results of the global simulations

3.1 Aerosol scavenged fractions

Figure 3 shows a frequency plot of the aerosol mass and number scavenged fractions for the DIAG-FULL simulation as compared to the prescribed ratios of Stier et al.

(2005). Particularly for mixed phase clouds, the scavenged fractions are <0.1 for near to 50% of the occurrences for number scavenging, and thus deviate considerably from the prescribed ratios, which are implemented in the CTL simulation. As the clouds glaciate, the Bergeron-Findeisen process causes rapid growth of the few ice crystals at the expense of the cloud droplets, which reduces the cloud droplet number concentration, and hence results in lower scavenged fractions for simulation DIAG-FULL. For warm phase clouds, the Aitken and accumulation mode scavenged fractions for simulation DIAG-FULL are greater than the prescribed ratios for 75% of the scavenging events. For ice clouds, the scavenging of the coarse mode is greater than the prescribed ratio of 0.1 for near to 60% of the scavenging occurrences. Figure 3 also shows that the scavenged fractions for the mass distributions are higher than for the number distributions. This is physically correct since the median radii of the aerosol mass distributions are higher than for the respective number distributions, and so mass distributions should be scavenged with higher fractions. As opposed to equating the mass with the number scavenging ratios, our approach will alter the aerosol size distribution to produce smaller aerosols. The impact of in-cloud scavenging on aerosol size is examined further in the following subsection.

Figure 4 shows the zonal and annual mean aerosol mass scavenged into the cloud droplets and ice crystals averaged over clear and cloudy regions, comparing the simulations CTL, DIAG-FULL, and PROG-AP. The scavenged fractions are greatest near the surface sources of the aerosols where warm phase clouds occur. In these regions, there are generally differences of <10% for the DIAG-FULL relative to the CTL simulation, but there are reductions of up to 50% for sulfate and sea salt scavenged mass over the southern oceans. For the PROG-AP simulation, scavenged fractions for all aerosol species in the regions of warm clouds are lower by near to 50% compared to the CTL simulation. Hoose et al. (2008a) explained this is a result of dependence of scavenged fraction on cloud history in an aerosol processing simulation. Alternatively, for the diagnostic and prescribed fraction scavenging approaches, all of the aerosol is assumed to be available for scavenging at each time-step since the in-droplet and in-crystal aerosol

ACPD
9, 22041–22101, 2009

concentrations are not passed between model time-steps. Both the DIAG-FULL and PROG-AP simulation behave similarly in the colder regions of the troposphere where mixed and ice phase clouds occur. The scavenged fractions are more than two times greater than for the CTL simulation. To correctly interpret these differences one must remember that these scavenged mass fractions are function of the cloud cover, the total aerosol concentration, and the number of cloud droplets and ice crystals. Relative to the CTL simulation, regions where aerosol concentrations are greater tend to be associated with higher scavenged mass, and conversely lower aerosol concentrations are associated with lower scavenged masses. The aerosol mass scavenged into the cloud droplets and ice crystals may not necessarily be removed by precipitation, since the rates of formation of precipitation, and the evaporation rates also ultimately control the aerosol mass that is removed from the atmosphere.

For the simulation PROG-AP, the mass transfer rates between the interstitial and in-droplet and in-crystal modes are shown in Fig. 5. This figure is similar to that shown in Hoose et al. (2008a). However, for this study we have used a more recent model version, and our dust and sea salt emissions are different with nudged meteorological conditions as compared to Hoose et al. (2008a). Similar to Hoose et al. (2008a), cloud droplet nucleation is a dominant process for transfer to aerosol mass into the in-droplet mode. Our results differ in that collisions are shown to dominate over nucleation or freezing for transfer of aerosol into the ice crystals. This is in agreement with recent work by Baumgardner et al. (2008), who suggested that impaction scavenging might dominate over nucleation scavenging for black carbon scavenging into ice crystals. Our study also implemented the below-cloud scavenging parameterization of Croft et al. (2009), which accounts for the higher removal of the interstitial aerosols by below-cloud scavenging in comparison to the results in Fig. 6 of Hoose et al. (2008a).

3.2 Impacts on aerosol size distributions

Figure 6 shows the zonal and annual mean count median radius for the CTL simulation, and the percent difference for the simulations DIAG2 relative to DIAG1, and also

for the simulations DIAG-FULL and PROG-AP relative to the CTL. As opposed to using the same scavenging ratios for the aerosol mass and number distributions (simulation DIAG1), the implementation of separate mass and number scavenging ratios gives annual and zonal mean soluble accumulation and coarse mode count median radii that are smaller by up to 40% and 50%, respectively (simulation DIAG2). The regions of mixed and ice phase clouds in the middle and upper troposphere show the greatest sensitivity for the count median aerosol radius to the implementation of separate scavenging ratios for aerosol mass and number distributions. This sensitivity is not as great for the near surface warm phase clouds since warm phase clouds had mass and number scavenging ratios of near to unity for the soluble/internally mixed accumulation and coarse modes in more than 90% of the scavenging occurrences (see Fig. 3). Figure 6 shows that the soluble/internally mixed Aitken mode radius does not change by more than 10% with the implementation separate mass and number nucleation scavenging ratios. This lower sensitivity is expected since the number of occurrences of nucleation scavenging for the soluble Aitken mode is nearly one order of magnitude smaller as compared to the larger soluble/internally mixed accumulation and coarse modes.

Figure 6 also shows how the zonal and annual mean count median radius is changed for the simulations DIAG-FULL and PROG-AP as compared to the CTL simulation. For the DIAG-FULL simulation, the zonal and annual mean soluble accumulation and coarse mode count median radii are reduced by up to 50% in regions of mixed and ice phase clouds, but the soluble Aitken mode radius is increased by up to 30%. Conversely, for the PROG-AP simulation the zonal and annual soluble accumulation and coarse mode radii are increased by near to 100% throughout much of the lower and middle troposphere. This increased radius is typical for prognostic aerosol cloud processing simulations, which include the process of coagulation of in-droplet and in-crystal aerosols followed by evaporation or sublimation. This is associated with the release of larger aerosol particles to the atmosphere (Hoose et al., 2008a).

ACPD
9, 22041–22101, 2009

3.3 Impacts on aerosol mass distributions

The zonal and annual mean aerosol mass mixing ratios comparing the simulations CTL, DIAG-FULL and PROG-AP are shown in Fig. 7. Both the DIAG-FULL and the PROG-AP simulations show an increase in dust and carbonaceous aerosol mass by more than five-fold towards the poles, and at the altitudes of mixed phase clouds, in comparison to the CTL simulation. The insoluble modes that contain dust and carbon aerosols are not scavenged by nucleation, and this contributes to the mass increase. However, sulfate and sea salt mass are increased by near to two-fold towards the poles and in the mixed phase clouds. The lower number of cloud droplets as the clouds glaciate and hence reduced nucleation scavenging contributes to this mass increase. For the DIAG-FULL simulation, the higher impaction scavenging of the accumulation and coarse modes aerosols in the ice clouds as compared to the PROG-AP and CTL simulations contributes to the relatively lower concentrations of dust and sea salt in the upper troposphere.

Table 4 presents the annual and global mean mass burdens and lifetimes for the five aerosol species, and for all the simulations conducted. The aerosol mass burdens are lower for the simulation DIAG-FULL, by 7%, 2%, 16%, and 30% for sulfate, particulate organic matter, dust, and sea salt, respectively, as compared to the PROG-AP simulation. Similarly, Ghan and Easter (2006) showed that a diagnostic scavenging scheme under-estimated aerosol burdens by near to 20% as compared to a prognostic treatment of in-droplet aerosol. Aerosols are kept within the cloud droplets and ice crystals between time-steps for the prognostic aerosol processing simulation, and this affects the mass and number of aerosols available for scavenging into the cloud droplets and crystals at each time-step, and ultimately the mass distribution. For our study, the black carbon mass burden increased by 2% for the simulation DIAG-FULL relative to PROG-AP. This results from black carbon burden sensitivity to differences in the representation of in-cloud impaction scavenging.

The simulation F100 allows us to compare the prescribed ratio approach of Stier

ACPD
9, 22041–22101, 2009

et al. (2005) with the more simplistic assumption that 100% of the aerosols in clouds are in the droplets and crystals. This simplistic approach has been used in global models (Barth et al., 2000). We find that the global and annual mean aerosol mass burdens in simulation F100 are lower in comparison to the CTL simulation, by up to 10% for sulfate. The greatest mass burden difference between all simulations was 32% for the global and annual mean sea salt burden, between the F100 simulation and the PROG-AP simulations. Assuming that only the soluble/internally mixed aerosols are cloud-borne for the simulation F100-INT as compared to F100 does not affect the sulfate and sea salt burdens significantly, since these aerosols do not exist in the insoluble modes. However, the annual and global mean black carbon and dust burdens are higher by near to 10% when none of the insoluble aerosols are allowed to be cloud-borne.

Comparing the simulations DIAG1 and DIAG2 illustrates the impact of diagnosing separate stratiform nucleation scavenging ratios for aerosol mass and number distributions. The global and annual mean mass burdens are higher by near to 10% and 8% for sulfate and carbonaceous aerosols, and 5% for sea salt and dust for the simulation DIAG1 as compared to DIAG2, which diagnoses separate mass and number scavenging ratios.

Table 4 also includes two simulations with the in-cloud impaction processes turned off, DIAG-FULL-noimp and PROG-AP-noimp. In comparing these two simulations with DIAG-FULL and PROG-AP, respectively, impaction scavenging is found to have a greater influence on the mass burdens in the case of prognostic aerosol cloud processing, and particularly for the aerosol species that occur in the submicrometer size modes. The annual and global mean sulfate mass, and black carbon burdens were reduced by 22% and 30%, respectively, for the PROG-AP simulation as compared to PROG-AP-noimp.

3.4 Impacts on aerosol number distributions

Figure 8 shows the geographic distribution of the ratio of the number burdens between the F100, DIAG-FULL, and PROG-AP simulations, and the CTL simulation. For the

PROG-AP simulation only the interstitial number burdens are shown. The accumulation mode number burdens in the DIAG-FULL and PROG-AP simulations increase by near to 2 and 5 times, respectively, as compared to the CTL in the regions of greater stratiform cloud cover, poleward of 30°. Ghan and Easter (2006) also found accumulation mode number burdens higher by up to two times towards the poles for a prognostic as compared to diagnostic in-cloud aerosol scavenging treatment. For the F100 simulation, the accumulation mode number burdens are lower by up to 20% over the regions of stratiform cloud cover in comparison to the CTL simulation. The nucleation and internally mixed/soluble Aitken mode number burdens are reduced by up to 50% poleward of 30° for the DIAG-FULL simulation. Comparing the DIAG2 and DIAG-FULL simulations (not shown) indicated the size-dependent aerosol scavenging impaction contributed largely to this burden reduction. For the F100 simulation, the nucleation number burdens are significantly increased by up to five times over the polar regions in comparison to the CTL simulation. Despite the increased in-cloud scavenging coefficients used in F100, the reduction in surface area available for sulfate condensation on to the larger aerosol modes leads to an increase in new particle formation. The annual and global mean new particle nucleation rate was nearly three times greater for the F100 simulation as compared to the DIAG-FULL simulation. For the PROG-AP simulation, the interstial coarse mode is reduced by up to half over the southern oceans. This occurs since the in-droplet and in-crystal modes (not shown here) contain these aerosols.

Table 5 summarizes the global and annual mean number burdens of the seven standard modes of the ECHAM5-HAM. For the DIAG-FULL simulation, the nucleation and internally mixed/soluble Atiken mode number burdens are decreased by 11% and 30%, respectively relative to the CTL simulation. Comparing these results for the simulations DIAG2 and DIAG-FULL, we can see that the new size-dependent impaction parameterization used in simulation DIAG-FULL has contributed to this change. For the DIAG-FULL simulation, the soluble/internally mixed Aitken and accumulation mode number burdens are 15% smaller compared to PROG-AP. For the PROG-AP simulation rela-

ACPD
9, 22041–22101, 2009

tive to the CTL, the number of internally mixed/soluble Aitken mode aerosols is reduced by near to 15%, and the internally mixed/soluble accumulation mode numbers are increased by near to 45%. Changes in the Aitken and accumulation mode numbers are relevant since these sizes are the most radiatively active. Ghan and Easter (2006) showed that smaller changes in global aerosol burdens (near to 20%) changed the magnitude of the direct and indirect radiative forcing of aerosols on climate by considerably less than the magnitude of the current uncertainty asociated with this forcing. This uncertainty arises from numerous, additional sources, including the representation of aerosol activation and cloud droplet spectra, limitations of model resolution, and lack of knowledge of pre-industrial aerosol emissions (IPCC, 2007).

3.5 Impacts on aerosol wet deposition

The geographic distribution of wet deposition for the five aerosol species is shown in Fig. 9. For the species that exist only in the soluble/internally mixed modes, sea salt and sulfate, there is very little change to the geographic distribution of wet deposition for the DIAG-FULL simulation as compared to the CTL. For the DIAG-FULL simulation, dust and the carbonaceous aerosol wet deposition is generally changed by less than 10% close to the major source regions, but increases poleward and over the more remote oceans by near to 100%. Over these more remote regions, these aerosols will have aged into the soluble/internally mixed modes, which are scavenged by cloud droplet and ice nucleation. However, the magnitude of the wet deposition is quite small in these regions. For the PROG-AP simulation, there are reductions in the wet deposition of sulfate and carbonaceous aerosols near to 25% close to the source regions. The total precipitation, which is also shown in Fig. 9 does not change significantly between simulations, and so these differences in wet deposition occur in response to the changes to the in-cloud scavenging parameterization, as opposed to changes to the rate of precipitation.

3.6 Aerosol deposition budgets

Tables 6–10 summarize the deposition budgets for the five aerosol species. For the DIAG-FULL simulation, in-cloud scavenging accounts for near to 80% of the total removal of sulfate and carbonaceous aerosols, and close to 35% of the total removal of sea salt and dust. Stratiform, as opposed to convective, in-cloud scavenging accounts for near to 65% of the total removal of sea salt and sulfate, but nearer to 40% of the total removal of carboneous aerosols and dust, which have greater sources towards the tropics. Removal by warm phase nucleation (temperatures >273.15 K) is about twice that of mixed phase nucleation (temperatures between 273.15 K and 238.15 K) for sulfate and the carbonaceous aerosols, whereas for sea salt and dust these processes are nearly equivalent. For simulation DIAG-FULL, nucleation scavenging accounts for 98%, 94%, 96%, 51%, and 99% of the total deposition due to stratiform in-cloud scavenging for sulfate, black carbon, particulate organic matter, dust, and sea salt, respectively. The remainder is due to in-cloud impaction scavenging. Below-cloud scavenging accounts for 13%, 14%, 11%, 25%, and 23% of the total annual and global mean deposition of sulfate, black carbon, particulate organic matter, dust, and sea salt, respectively for the simulation DIAG-FULL.

The contribution of impaction scavenging to total deposition can be examined for the diagnostic scavenging simulations. For dust and sea salt, which reside only in the accumulation and coarse modes, the global and annual mean removal by impaction in warm and mixed phase clouds is increased by near to 2 orders of magnitude in the simulation DIAG-FULL, which has physically detailed size-dependent in-cloud impaction scavenging, as compared to DIAG2, which implements the prescribed impaction scavenging kernels of Hoose et al. (2008a). The global and annual mean dust mass burden (see Table 4) is decreased by near to 6% in simulation DIAG-FULL as compared to DIAG2. The sea salt burden does not change significantly, since impaction contributes <1% to the total sea salt removal. For sulfate, the global mean impaction scavenging is near to two times greater in warm and mixed phase clouds for the simulation DIAG-FULL

ACPD
9, 22041–22101, 2009

as compared to DIAG2, but the mass burden is not significantly changed. For black carbon, and particulate organic matter, the impaction scavenging is reduced by about half in DIAG-FULL as compared to DIAG2, and the respective burdens are increased by 8% and 3%. Impaction scavenging contributes relatively more to the total deposition for black carbon since a greater fraction of the black carbon (80%) is emitted into the insoluble mode, as opposed to 50% for particulate organic matter. The soluble/internally mixed Aitken mode number burden is reduced by 20% for the DIAG-FULL simulation as compared to the DIAG2 simulation. Our results suggest that for modeling of dust and black carbon mass, and sub-micron size particle number burdens, some consideration should be given to the representation of in-cloud impaction in global models.

For the simulation PROG-AP compared to the CTL simulation, the total aerosol removal by in-cloud scavenging is reduced by 20 to 25% for all aerosol species, with the greatest changes for sulfate and sea salt, with a sea salt mass burden increase of 35%. Increased aerosol burden for prognostic aerosol cloud processing simulations have been shown by Hoose et al. (2008a) and Ghan and Easter (2006). The aerosol load that remains in the stratiform cloud droplets is not available for the convective scavenging, and so the convective in-cloud scavenging is also reduced by near to 10% for sulfate. Only dust is affected in the opposite sense and the convective scavenging is actually increased by a few percent. This is expected since stratiform in-cloud scavenging of dust is a less important sink compared to other removal processes, and Fig. 1 shows that the Hoose et al. (2008a,b) impaction scheme also scavenges coarse mode particles, such as dust, into the cloud droplets relatively inefficiently. These results point to the relevance of developing a convective aerosol processing treatment in the future that should be coupled with the stratiform aerosol processing treatment of Hoose et al. (2008a,b).

4 Comparison with observations

Figures 10 and 11 show the comparison of the modeled wet deposition of sulfate with the observations compiled by Dentener et al. (2006a), and grouped according to geographic region. The simulations DIAG-FULL and PROG-AP compare similarly to the observations relative to the CTL simulation. However, the correlation coefficient and slope are overall slightly improved for the PROG-AP simulation as compared to the other simulations for the global mean, National Atmospheric Deposition Program (NADP), India and African (IDAF) datasets. For all simulations, the modeled deposition is within a factor of two of the observations for at least 75% of the sites. The PROG-AP simulation does not perform as well as the CTL or DIAG-FULL simulation for the European (EMEP), and the East Asian (EANET) datasets, with a reduction in the correlation coeffients, but only by a few percent. Futures improvement to the prognostic aerosol cloud processing scheme, including introduction of a convective aerosol cloud processing scheme, and implementing size-dependent impaction scavenging together with the aerosol processing approach could improve the agreement with observations.

Figure 12 shows the geographic distribution of aerosol optical depth (AOD) for the years 2001–2006, created from a combination of MODIS (Levy et al., 2007) and MISR (Diner et al., 2005; Martonchik et al., 2002) retrievals, as described in van Donkelaar et al. (2009). The composite MODIS and MISR dataset is created from the ensemble of individual retrievals that exhibit little bias versus ground-based AERONET (Holben et al., 1998) AOD observations. More specifically, the accuracy of the MODIS and MISR AOD retrieval over land is evaluated relative to AERONET AOD on a monthly basis for nine land types defined using the MODIS BRDF/Albedo product at three different wavelengths (470 nm, 660 nm and 2.1 μm). Daily MODIS and MISR AOD retrievals over land types that exhibit a mean monthly bias in excess of either 0.1 or 20% are rejected. The remaining retrievals over 2001–2006 are averaged. The composite dataset is driven by MISR observations over bright surfaces where MODIS is biased (Abdou et al., 2005), and over dark surfaces by MODIS (higher temporal sampling).

ACPD
9, 22041–22101, 2009

MODIS AOD is used over the ocean due to high sampling frequency and accuracy (Remer et al., 2005). Annual mean AOD enhancements of >0.5 reflect a combination of mineral dust over and downwind of Africa, as well as large anthropogenic signals over India and East Asia. Sea salt contributes to moderate AOD enhancements at southern high latitudes.

Figure 12 also shows the geographic distribution of the ratio of the aerosol optical depth (AOD) for the simulations CTL, DIAG-FULL, and PROG-AP compared to the observational dataset. Both the DIAG-FULL and CTL simulations perform similarly. The number of grid points within 25% of the observations is increased by near to 20% over the oceans for the DIAG-FULL simulation as compared to the CTL. The PROG-AP simulation has slightly lower AODs (10 to 20%) over the land, which improves the agreement with observations over eastern North America and Europe, but the AOD is under-predicted over Asia, and considerably over-predicted over the oceans (up to a factor of two). Hoose et al. (2008a) have shown that the agreement over the oceans can be improved with changes to the water uptake on the aerosols, which will be implemented in future versions of the ECHAM5-HAM.

Hoose et al. (2008a) showed that a prognostic in-cloud scavenging scheme modified zonal mean aerosol size distributions in the marine boundary layer to produce better agreement with the observations of Heintzenberg et al. (2000), particularly for the accumulation mode. These observations are shown in Fig. 13. The observations of Heintzenberg et al. (2000) are a compilation of data from different mobility, and aerodynamic sizing techniques, operated at relative humidities of <40%, and a multi-modal lognormal distribution was fitted to the observations. The same methodology as described in Hoose et al. (2008a) was used for comparision with the simulations CTL, DIAG-FULL, and PROG-AP. Figure 13 shows that the DIAG-FULL simulation, unlike the PROG-AP simulation, does not modify the marine accumulation mode size distribution significantly as compared to the CTL simulation. The Aitken mode number concentrations are under-estimated by up to five times over the southern oceans for all simulations in comparison to the observations. A considerable reduction in the under-

estimation could be made with changes to the treatment of new particle formation in the marine boundary layer, which will be implemented in future ECHAM versions. For the DIAG-FULL simulation, the Aitken mode numbers are reduced by half in the Southern Hemisphere relative to the CTL simulation, which is a consequence of the more vigorous scavenging in the marine boundary layer for the diagnostic scheme.

Recently Koch et al. (2009) presented black carbon profiles observed from aircraft in comparison to various global models. Figures 14 and 15 compare this same aircraft data with our model simulations, CTL, DIAG-FULL, and PROG-AP. Additionally we have included two sensitivity simulations that have the in-cloud impaction processes turned off for both the diagnostic and prognostic in-cloud scavenging schemes, DIAG-FULL-noimp and PROG-AP-noimp, respectively. These figures show that the black carbon profiles particularly in the middle troposphere can vary by up to two orders of magnitude depending on the treatment of in-cloud scavenging. This effect is more pronounced for the more northerly profiles shown in Fig. 15, where mixed phase and ice clouds are more prevalent. For the simulation PROG-AP as compared to PROG-AP-noimp, black carbon concentrations are lower by up to a factor of five, and two in the middle and upper troposphere, respectively. This points to the importance of the parameterization of impaction scavenging of black carbon for mixed and ice clouds. For seven of the ten of the profiles presented, the black carbon profile is closer to the observations for the DIAG-FULL and PROG-AP simulations as compared to the CTL simulation (changes up to one order of magnitude). For the three profiles of Fig. 14 that show closer agreement with observations for the prescribed coefficient scheme of the CTL simulation, the PROG-AP simulation is a better match to the observations than for the DIAG-FULL simulation.

4.1 Simulation of ^{210}Pb and ^{7}Be

^{7}Be and ^{210}Pb have been simulated in global models, and used as passive tracers for the validation of deposition parameterizations (e.g., Brost et al., 1991; Liu et al., 2001; Feichter et al., 1991; Koch et al., 1996, 2006). Recently, simulation of ^{7}Be and

^{210}Pb have been introduced into the ECHAM5-HAM (Heikkilä et al., 2008, 2009). The methodology is described in detail in Feichter et al. (1991); Heikkilä (2007); Heikkilä et al. (2008). These tracers have been coupled with the CTL and DIAG-FULL simulations. Figure 16 compares the surface layer concentrations and wet deposition of these tracers for the simulations CTL and DIAG-FULL with the observations. The comparison with observed surface layer concentrations and wet deposition is most robust for ^{210}Pb since ^{210}Pb originates from surface sources and rarely reaches the stratosphere. ^{210}Pb has a relatively long half-life with respect to radioactive decay processes (22.4 years), but a relatively short atmospheric residence time (3–5 days) due to wet deposition processes. Conversely, the ^{7}Be source is in the upper atmosphere and ^{7}Be has a shorter half-life (few months). The longer transport path from source to the cloud levels or surface, coupled with the shorter half-life, increases the uncertainty associated with comparisons between the modeled and observed deposition and surface layer concentrations for ^{7}Be. Nevertheless, Fig. 16 shows that both tracers are simulated reasonably in comparison with observations of deposition and surface layer concentrations. Unfortunately, the quality of deposition observations available is not optimal. The observed surface layer concentrations are 10–30 year means, and the deposition fluxes are 1–5 year means. The deposition observations are older, mostly taken from 1980s and 1990s and do not have a global coverage as extensive as the surface layer concentration observations. As a result of these factors, the best correlation coefficients, slope and offset parameters are for the case of ^{210}Pb surface layer concentrations. However, for both deposition and surface layer concentration, the DIAG-FULL and CTL simulations are within a factor of two of the observations at more than 75% of the sites. The correlation coefficients are improved by a few percent for the DIAG-FULL simulation as compared to the CTL simulation for both the ^{210}Pb surface layer concentration and wet deposition.

5 Summary and conclusions

A nucleation scavenging scheme that diagnoses cloud scavenging ratios for aerosol mass and number distributions based on cloud droplet and ice crystal number concentrations has been coupled with a physically detailed size-dependent in-cloud impaction scavenging parameterization, and implemented for stratiform clouds in the ECHAM5-HAM model. The global and annual mean aerosol mass burdens increased by 8% for carbonaceous aerosols, 3% for sulfate and dust, and decreased 3% for sea salt compared to a simulation using the prescribed in-cloud scavenging ratios of the standard ECHAM5-HAM. The soluble/internally mixed Aitken and accumulation mode number burdens were decreased by 30%, and increased by 25%, respectively, relative to the prescribed scavenging ratio simulation. Annual and global mean sea salt and dust burdens were decreased by 30% and 15%, respectively for a simulation with the new diagnostic scavenging as compared to a simulation with the prognostic aerosol cloud processing scheme of Hoose et al. (2008a,b). Assuming that 100% of the in-cloud aerosol is scavenged into the cloud droplets and ice crystals gave the maximum burden change in this study, and reduced the global annual mean sea salt mass and accumulation mode number burdens by 32% and 65%, respectively, relative to a simulation with prognostic aerosol processing. This is more than the maximum change of 20% reported by Ghan and Easter (2006) who compared prognostic and diagnostic scavenging approaches. A physically detailed in-cloud impaction scavenging parameterization was shown to reduce the global and annual mean dust mass, and the soluble Aitken mode number burdens by near to 6% and 17%, respectively, and increase the black carbon mass burden by 8%, relative to an otherwise similar simulation that used the Hoose et al. (2008a,b) prescribed collection kernels for each aerosol mode. For the prognostic scheme, implementation of impaction scavenging reduced the black carbon burden by 30%. Thus, particularly for dust and black carbon mass, and submicrometer-size mode number burdens, some consideration should be given to the representation of in-cloud impaction scavenging in global models.

ACPD
9, 22041–22101, 2009

In comparison with observations of wet deposition and aerosol optical depth, the new diagnostic scheme was found to perform similarly, or slightly better than the prescribed scavenging coefficient approach of Stier et al. (2005). We have presented a new aerosol optical depth climatology (2001–2006) produced from a combination of MODIS, MISR, and AERONET observations, and have used this to evaluate our simulations. The prescribed scavenging ratio scheme of the standard ECHAM5-HAM under-estimated black carbon profiles observed from aircraft by up to two orders of magnitude. The revised diagnostic and prognostic scavenging schemes improved the agreement to within one order of magnitude.

The prognostic aerosol cloud processing scheme used for this study does require 10 additional tracers, and thus diagnostic scavenging schemes can be desirable in global models due their relative simplicity. However, prognostic aerosol processing schemes, such that of Hoose et al. (2008a,b) are beneficial, and future work should be directed towards extending this prognostic approach to convective clouds, particularly since convective scavenging does account for near to 50% of global wet scavenging. Future studies should also examine the implementation of separate mass and number scavenging ratios for the stratiform aerosol processing scheme of the ECHAM5-HAM. The global annual mean sulfate and carbonaceous aerosol mass burdens increased by 10% for the diagnostic scheme when the mass and number scavenging ratios were equated, as opposed to determined separately. Finally, future work could be directed towards examining the influence of these various in-cloud scavenging parameterizations, which have been shown to influence aerosol size distributions, on the aerosol direct and indirect effects upon the climate system.

Acknowledgements. The authors are grateful to the National Science and Engineering Research Council of Canada and Killam Trusts Foundation of Canada for financial support. We thank D. Koch, and the following groups associated with providing aircraft data: NOAA at UC Boulder (David Fahey), University of Tokyo (Y. Kondo), and University of Hawaii (T. Clarke). Thanks also to CSCS for computing time.

References

Abdou, W. A., Diner, D. J., Matonchik, J. V., Bruegge, C. J., Kahn, R. A., Gaitley, B. J., Crean, K. A., Remer, L. A., and Holben, B.: Comparison of coincident Multiangle Imaging Spectroradiometer aerosol optical depths over land and ocean scenes containing Aerosol Robotic Network sites, J. Geophys. Res., 110, D10S07, doi:10.1029/2004JD004693, 2005. 22064

Adams, P. J. and Seinfeld, J. H.: Predicting global aerosol size distributions in general circulation models, J. Geophys. Res., 107, 4370, doi:10.1029/2001JD001010, 2002. 22044

Barth, M., Rasch, P. J., Kiehl, J. T., Benkovitz, C. M., and Schwartz, S. E.: Sulfur chemistry in the NCAR CCM: Description, evaluation, features and sensitivity to aqueous chemistry, J. Geophys. Res., 105, 1387–1415, 2000. 22044, 22054, 22059

Baumgardner, D., Subramanian, R., Twohy, C., Stith, J., and Kok, G.: Scavenging of black carbon by ice crystals over the northern Pacific, Geophys. Res Lett., 35, L22815, doi:10.1029/2008GL035764, 2008. 22045, 22056

Brost, R., Feichter, J., and Heimann, M.: Three-dimensional simulation of ^{7}Be in a Global Climate Model, J. Geophys. Res., 96(D12), 22423–22445, 1991. 22066

Cagnazzo, C., Manzini, E., Giorgetta, M. A., Forster, P. M. De F., and Morcrette, J. J.: Impact of an improved shortwave radiation scheme in the MAECHAM5 General Circulation Model, Atmos. Chem. Phys., 7, 2503–2515, 2007, http://www.atmos-chem-phys.net/7/2503/2007/. 22046

Charlson, R. J., Schwartz, S. E., Hales, J. M., Cess, R. D., Coakley, J. A., Hansen, J. E., and Hofmann, D. J.: Climate forcing by anthropogenic aerosols., J. Geophys. Res., 255, 423–430, 1992. 22044

Chin, M., Rood, R. B., Lin, S.-J., Muller, J.-F., and Thompson, A. M.: Atmospheric sulfur cycle in the global model GOCART: Model description and global properties, J. Geophys. Res., 105, 24661–24687, 2000. 22044

Croft, B., Lohmann, U., Martin, R. V., Stier, P., Wurzler, S., Feichter, J., Posselt, R., and Ferrachat, S.: Aerosol size-dependent below-cloud scavenging by rain and snow in the ECHAM5-HAM, Atmos. Chem. Phys., 9, 4653–4675, 2009, http://www.atmos-chem-phys.net/9/4653/2009/. 22047, 22052, 22053, 22056

Dentener, F., Drevet, J., Lamarque, J. F., Bey, I., Eickhout, B., Fiore, A. M., Haiglustaine, D., Horowitz, L. W., Krol, M., Lawrence, U. C., Galy-Lacaux, C., Rast, S., Shindell, D., Stevenson, D., Noije, T. V., Atherton, C., Bell, N., Bergman, D., Butler, T., Cofala, J., Colins, B., Doherty,

R., Ellingsen, K., Galloway, J., Gauss, M., Montanaro, V., Müller, J. F., Pitari, G., Rodriguez, J., Sanderson, M., Solomon, F., Strahan, S., Schultz, M., Sudo, K., Szopa, S., and Wild, O.: Nitrogen and sulfur deposition on regional and global scales: A multimodel evaluation, Global Biogeochem. Cy., 20, GB4003,doi:10.1029/2005GB002672, 2006a. 22064, 22095, 22096

Dentener, F., Kinne, S., Bond, T., Boucher, O., Cofala, J., Generoso, S., Ginoux, P., Gong, S., Hoelzemann, J. J., Ito, A., Marelli, L., Penner, J. E., Putaud, J.-P., Textor, C., Schulz, M., van der Werf, G. R., and Wilson, J.: Emissions of primary aerosol and precursor gases in the years 2000 and 1750 prescribed data-sets for AeroCom, Atmos. Chem. Phys., 6, 4321–4344, 2006b. 22047

Diner, D. D., Braswell, B. H., Davies, R., Gobron, N., Hu, J., Jin, Y., Kahn, R. A., Knyazikhin, Y., Loeb, N., Muller, J.-P., Nolin, A. W., Pinty, B., Schaaf, C. B., Seiz, G., and Stroeve, J.: The value of multiangle measurements for retrieving structurally and radiatively consistent properties of cloud, aerosols and surfaces, Remote Sens. Environ., 97, 495–518, 2005. 22064

Feichter, J., Brost, R. A., and Heimann, M.: Three-dimensional modeling of the concentration and deposition of ^{210}Pb aerosols, J. Geophys. Res., 96(D12), 22447–22460, 1991. 22066, 22067

Ghan, S. J. and Easter, R. C.: Impact of cloud-borne aerosol representation on aerosol direct and indirect effects, Atmos. Chem. Phys., 6, 4163–4174, 2006, http://www.atmos-chem-phys.net/6/4163/2006/. 22044, 22045, 22058, 22060, 22061, 22063, 22068

Ghan, S. J., Chuang, C. C., and Penner, J. E.: A parameterization of cloud droplet nucleation part I: single aerosol type, Atmos. Res., 30, 198–221, 1993. 22048

Gong, S. L., Barrie, L. A., Blanchet, J.-P., vonSalzen, K., Lohmann, U., Lesins, G., Spacek, L., Zhang, L. M., Girard, E., Lin, H., Leaitch, R., Leighton, H., Chylek, P., and Huang, P.: Canadian Aerosol Module: A size-segregated simulation of atmospheric aerosol processes for climate and air quality models: 1. Module developments, J. Geophys. Res., 108, 4007, doi:10.1029/2001JD002002, 2003. 22044, 22045

Heikkilä, U.: Modeling of the atmospheric transport of the cosmogenic radionuclides ^{10}Be and ^{7}Be using the ECHAM5-HAM General Circulation Model, PhD thesis, Dissertation ETH No. 17516, online available at: http://e-collection.ethbib.ethz.ch, 2007. 22067

Heikkilä, U., Beer, J., and Feichter, J.: Modeling cosmogenic radionuclides ^{10}Be and ^{7}Be during

the Maunder Minimum using the ECHAM5-HAM General Circulation Model, Atmos. Chem. Phys., 8, 2797–2809, 2008, http://www.atmos-chem-phys.net/8/2797/2008/. 22067

Heikkilä, U., Beer, J., and Feichter, J.: Meridional transport and deposition of atmospheric ^{10}Be, Atmos. Chem. Phys., 9, 515–527, 2009, http://www.atmos-chem-phys.net/9/515/2009/. 22067

Heintzenberg, J., Covert, D. C., and van Dingenen, R.: Size distributions and chemical composition of marine aerosols: a composition and review, Tellus, 52B, 1104–1122, 2000. 22065, 22098

Holben, B. N., Eck, T. F., Slutsker, I., Tanre, D., Buis, J. P., Setzer, A., Vermote, E., Reagan, J. A., Kaufman, Y. J., Nakajima, T., Lavenu, F., Jankowiak, I., and Smirnov, A.: AERONET - A federated instrument network and data archive for aerosol characterization., Remote Sens. Environ., 66, 1–16, 1998. 22064

Hoose, C., Lohmann, U., Bennartz, R., Croft, B., and Lesins, G.: Global simulations of aerosol processing in clouds, Atmos. Chem. Phys., 8, 6939–6963, 2008a. 22044, 22045, 22053, 22054, 22055, 22056, 22057, 22062, 22063, 22065, 22068, 22069, 22077, 22078, 22086, 22087, 22098

Hoose, C., Lohmann, U., Stier, P., Verheggen, B., and Weingartner, E.: Aerosol processing in mixed-phase clouds in ECHAM5-HAM: Model description and comparison to obserations, J. Geophys. Res., 113, D07210, doi:10.1029/2007JD009251, 2008b. 22044, 22045, 22053, 22054, 22063, 22068, 22069, 22077, 22078, 22086, 22087

IPCC: Intergovernmental Panel on Climate Change: Climate Change 2007: The Physical Basis, edited by: Solomon, S., Qin, D., Manning, M., Marquis, M., Averyt, K., Tignor, M. M. B., Miller, H. L., and Chen, Z., Cambridge Univ. Press, Cambridge, UK, 2007. 22061

Koch, D., Jacob, D., and Graustein, W.: Vertical transport of tropospheric aerosols as indicated by ^{7}Be and ^{210}Pb in a chemical tracer model, J. Geophys. Res., 101(D13), 18651–18666, 1996. 22066

Koch, D., Schmidt, G. A., and Field, C. V.: Sulfur, sea salt, and radionuclide aerosols in GISS ModelE, J. Geophys. Res., 111, D12209, doi:10.1029/2005JD006899, 2006. 22066

Koch, D., Schulz, M., Kinne, S., Bond, T. C., Balkanski, Y., Bauer, S., Berntsen, T., Boucher, O., Chin, M., Clarke, A., De Luca, N., Dentener, F., Diehl, T., Dubovik, O., Easter, R., Fahey, D. W., Feichter, J., Fillmore, D., Freitag, S., Ghan, S., Ginoux, P., Gong, S., Horowitz, L., Iversen, T., Kirkevåg, A., Klimont, Z., Kondo, Y., Krol, M., Liu, X., McNaughton, C., Miller,

R., Montanaro, V., Moteki, N., Myhre, G., Penner, J. E., Perlwitz, Ja., Pitari, G., Reddy, S., Sahu, L., Sakamoto, H., Schuster, G., Schwarz, J. P., Seland, Ø., Spackman, J. R., Stier, P., Takegawa, N., Takemura, T., Textor, C., van Aardenne, J. A., and Zhao, Y.: Evaluation of black carbon estimations in global aerosol models, Atmos. Chem. Phys. Discuss., 9, 15769–15825, 2009, http://www.atmos-chem-phys-discuss.net/9/15769/2009/. 22066, 22099, 22100

Levy, R. C., Remer, L. A., Mattoo, S., and Vermote, E. F.: Second-generation operational algorithm: Retrieval of aerosol properties over land from inversion of Moderate Resolution Imaging Spectroradiometer spectral reflectance, J. Geophys. Res., 112, D13211, doi:10.1029/2006JD007811, 2007. 22064

Lin, S. J. and Rood, R. B.: Multidimensional flux form semi-Lagrangian transport, Mon. Weather Rev., 124, 2046–2068, 1996. 22046

Liu, H., Jacob, D. J., Bey, I., and Yantosca, R. M.: Constraints from ^{210}Pb and ^{7}Be on wet deposition and transport in a global three-dimensional chemical tracer model driven by assimilated meteorolgical fields, J. Geophys. Res., 106, 12109–12128, 2001. 22066

Lohmann, U. and Kärcher, B.: First interactive simulations of cirrus clouds formed by homogeneous freezing in the ECHAM general circulation model, J. Geophys. Res., 107(D10), 4105, doi:10.1029/2001JD000767, 2002. 22046, 22051

Lohmann, U., Stier, P., Hoose, C., Ferrachat, S., Kloster, S., Roeckner, E., and Zhang, J.: Cloud microphysics and aerosol indirect effects in the global climate model ECHAM5-HAM, Atmos. Chem. Phys., 7, 3425–3446, 2007, http://www.atmos-chem-phys.net/7/3425/2007/. 22046, 22048

Lohmann, U., Spichtinger, P., Jess, S., Peter, T., and Sit, H.: Cirrus cloud formation and ice supersaturated regions in a global climate model, Environ. Res. Lett., 3, 1–11, 2008. 22052

Martin, J. J., Wang, P. K., and Pruppacher, H. R.: A theoretical determination of the efficiency with which aerosol particles are collected by simple ice crystal plates., J. Atmos. Sci., 37, 1628–1638, 1980. 22053

Martonchik, J. V., Diner, D. J., Crean, K. A., and Bull, M. A.: Regional aerosol retrieval results from MISR, IEEE T. Geosci. Remote, 40, 1520–1531, 2002. 22064

Miller, N. L. and Wang, P. K.: Theoretical determination of the efficiency of aerosol particle collection by falling columnar ice crystals., J. Atmos. Sci., 46, 1656–1663, 1989. 22053

Miller, N. L. and Wang, P. K.: A theoretical determination of the collection rates of aerosol particles by falling ice crystal plates and columns, Atmos. Environ., 25A, 2593–2606, 1991.

22052, 22053, 22087
Mlawer, E. J., Taubman, S. J., Brown, P. D., Iacono, M. J., and Clough, S. A.: Radiative transfer for inhomogeneous atmosphere: RRTM, a validated correlated-k model for the longwave, J. Geophys. Res., 102, 16663–16682, 1997. 22046
Morcrette, J.-J., Clough, S. A., Mlawer, E. J., and Iacono, M. J.: Impact of a validated radiative transfer scheme, RRTM, on the ECMWF model cliamte and 10-day forecasts, ECMWF, Reading, UK, technical memorandum 252 edn., 1998. 22046
Nordeng, T. E.: Extended versions of the convective parameterization scheme ay ECWMF and their impact on the mean and transient activity of the model in the tropics, ECMWF, Reading, UK, technical memorandum edn., 1994. 22046
Pruppacher, H. R. and Klett, J. D.: Microphysics of clouds and precipitation., Kluwer Academic Publishers, Dordrecht, Boston, London, 1997. 22044
Remer, L. A., Kaufman, Y. J., Tanre, D., Mattoo, S., Chu, D. A., Martins, J. V., Li, R.-R., Ichoku, C., Levy, R. C., Kleidman, R. G., Eck, T. F., Vermote, E., and Holben, B. N.: The MODIS aerosol algorithm, products and validation, J. Atmos. Sci., 62, 947–973, 2005. 22065
Roeckner, E., Baeuml, G., Bonventura, L., Brokopf, R., Esch, M., Giorgetta, M., Hagemann, S., Kirchner, I., Kornblueh, L., Manzini, E., Rhodin, A., Schlese, U., Schilzweida, U., and Tompkins, A.: The atmospheric general circulation model ECHAM5. Part I: Model description, Report 349, Max Planck Institute for Meteorology, Hamburg, Germany, online available at: http://www.mpimet.mpg.de, 2003. 22046
Spichtinger, P. and Gierens, K. M.: Modelling of cirrus clouds – Part 1a: Model description and validation, Atmos. Chem. Phys., 9, 685–706, 2009, http://www.atmos-chem-phys.net/9/685/2009/. 22053
Stier, P., Feichter, J., Kinne, S., Kloster, S., Vignati, E., Wilson, J., Ganzeveld, L., Tegen, I., Werner, M., Balkanski, Y., Schulz, M., Boucher, O., Minikin, A., and Petzold, A.: The aerosol-climate model ECHAM5-HAM, Atmos. Chem. Phys., 5, 1125–1156, 2005, http://www.atmos-chem-phys.net/5/1125/2005/. 22044, 22046, 22047, 22048, 22050, 22054, 22058, 22069, 22076, 22088
Takemura, T., Nakajima, T., Dubovik, O., Holben, B. N., and Kinne, S.: Single scattering albedo and radiative forcing of various aerosol species with a global three-dimensional model, J. Climate, 15, 333–352, 2002. 22044
Textor, C., Schulz, M., Guibert, S., Kinne, S., Balkanski, Y., Bauer, S., Berntsen, T., Berglen, T., Boucher, O., Chin, M., Dentener, F., Diehl, T., Easter, R., Feichter, H., Fillmore, D., Ghan, S.,

Ginoux, P., Gong, S., Grini, A., Hendricks, J., Horowitz, L., Huang, P., Isaksen, I., Iversen, I., Kloster, S., Koch, D., Kirkevåg, A., Kristjansson, J. E., Krol, M., Lauer, A., Lamarque, J. F., Liu, X., Montanaro, V., Myhre, G., Penner, J., Pitari, G., Reddy, S., Seland, Ø., Stier, P., Takemura, T., and Tie, X.: Analysis and quantification of the diversities of aerosol life cycles within AeroCom, Atmos. Chem. Phys., 6, 1777–1813, 2006, http://www.atmos-chem-phys.net/6/1777/2006/. 22044

Tie, X., Madronich, S., Walters, S., Edwards, D. P., Ginoux, P., Mahowald, N., Zhang, R. Y., Lou, C., and Brasseur, G.: Assessment of the global impact of aerosols on tropospheric oxidants, J. Geophys. Res., 110, D03204, doi:10.1029/2004JD005359, 2005. 22044

Tiedtke, M.: A comprehensive mass flux scheme for cumulus parameterization in large scale model, Mon. Weather Rev., 117, 1779–1800, 1989. 22046

Twomey, S.: Aerosol, clouds, and radiation., Atmos. Environ., 25A, 2435–2442, 1991. 22044

van Donkelaar, A., Martin, R. V., Brauer, M., Kahn, R., Levy, R., Verduzco, C., and Villeneuve, P.: Global estimates of average ground-level fine particulate matter concentrations from satellite-based aerosol optical depth, Environ. Health Persp., submitted, 2009. 22064, 22097

Table 1. In-cloud scavenging ratios for each of the seven log-normal modes of the ECHAM5-HAM dependent on the cloud type and temperature (warm: $T > 273.15$ K, mixed: $238.15 < T \leq 273.15$ K, ice: $T \leq 238.15$ K) following Stier et al. (2005).

Mode	Warm stratiform	Mixed stratiform	Ice stratiform	Convective
Nucleation soluble (NS)	0.10	0.10	0.00	0.20
Aitken soluble (KS)	0.25	0.40	0.10	0.60
Accumulation soluble (AS)	0.85	0.75	0.10	0.99
Coarse soluble (CS)	0.99	0.75	0.10	0.99
Aitken insoluble (KI)	0.20	0.10	0.10	0.20
Accumulation insoluble (AI)	0.40	0.40	0.10	0.40
Coarse insoluble (CI)	0.40	0.40	0.10	0.40

Table 2. In-cloud impaction scavenging kernels ($m^3\,s^{-1}$) for aerosol-droplet and aerosol-ice crystal collision for each of the seven log-normal modes of the ECHAM5-HAM following Hoose et al. (2008a,b).

Mode	Droplets	Crystals
Nucleation soluble (NS)	2.5×10^{-12}	5.0×10^{-11}
Aitken soluble (KS)	2.5×10^{-12}	5.0×10^{-11}
Accumulation soluble (AS)	2.0×10^{-14}	2.0×10^{-12}
Coarse soluble (CS)	0.0	2.0×10^{-13}
Aitken insoluble (KI)	2.5×10^{-12}	5.0×10^{-11}
Accumulation insoluble (AI)	2.0×10^{-14}	2.0×10^{-12}
Coarse insoluble (CI)	0.0	2.0×10^{-13}

ACPD
9, 22041–22101, 2009

Table 3. The simulations conducted for this study are summarized in this table.

Simulation	Description
CTL	Control simulation using prescribed in-cloud scavenging ratios from Table 1
F100	Assuming 100% of aerosols in clouds are cloud-borne for all aerosol modes
F100-INT	Assuming 100% of soluble/internally mixed aerosols in clouds are cloud-borne, and 0% of insoluble aerosols are cloud-borne
DIAG1	In-cloud scavenging ratios diagnosed from cloud droplet and ice crystal number concentrations, equating the mass with the number nucleation scavenging ratios, and using Hoose et al. (2008a,b) impaction scavenging kernels from Table 2
DIAG2	Same as DIAG1, but with separate mass and number nucleation scavenging ratios (see text for details)
DIAG-FULL	Same as DIAG2, but using physically detailed size-dependent in-cloud impaction scavenging coefficients, and kernels for cloud droplets and ice crystals shown in Figs. 1 and 2
DIAG-FULL-noimp	Same as DIAG-FULL except no in-cloud impaction scavenging
PROG-AP	Prognostic stratiform aerosol processing scheme of Hoose et al. (2008a,b)
PROG-AP-noimp	Same as PROG-AP except no in-cloud impaction scavenging

ACPD
9, 22041–22101, 2009

Table 4. Annual and global mean mass burdens (Tg, except Tg S for sulfate) and lifetimes (days) given in brackets immediately following the burdens, for the five aerosol species, and for the simulations described in Table 3. POM refers to particulate organic matter.

Burden (lifetime)	Sulfate	Black carbon	POM	Dust	Sea salt
CTL	0.843 (4.2)	0.119 (5.6)	1.04 (5.7)	3.60 (3.9)	8.28 (0.56)
F100	0.749 (3.7)	0.109 (5.2)	0.99 (5.4)	3.40 (3.7)	7.86 (0.53)
F100-INT	0.750 (3.7)	0.116 (5.5)	1.10 (6.1)	3.77 (4.1)	7.85 (0.53)
DIAG1	0.965 (4.8)	0.133 (6.3)	1.17 (6.5)	4.10 (4.3)	8.39 (0.57)
DIAG2	0.867 (4.3)	0.122 (5.8)	1.08 (6.0)	3.93 (4.2)	7.99 (0.54)
DIAG-FULL	0.886 (4.4)	0.132 (6.3)	1.11 (6.1)	3.69 (3.9)	7.95 (0.54)
DIAG-FULL-noimp	0.991 (4.6)	0.135 (6.4)	1.13 (6.2)	3.95 (4.2)	8.01 (0.54)
PROG-AP	0.952 (4.8)	0.129 (6.1)	1.13 (6.2)	4.41 (4.6)	11.4 (0.77)
PROG-AP-noimp	1.228 (6.1)	0.186 (8.8)	1.46 (8.1)	4.78 (5.0)	12.9 (0.87)

Table 5. Global and annual mean number burdens ($10^{10}\,m^{-2}$) for the nine simulations and for the seven aerosol modes. CD and IC refer to the in-droplet and in-crystal modes of the prognostic simulation. Abbreviations are defined in Tables 1 and 3.

Number	NS	KS	AS	CS	KI	AI	CI	CD	IC
CTL	18800.0	870.0	75.1	0.441	8.29	0.031	0.068		
F100	31500.0	1170.	65.9	0.414	6.84	0.028	0.063		
F100-INT	31500.0	1160.	67.0	0.430	8.69	0.047	0.081		
DIAG1	17600.0	668.0	87.2	0.476	8.12	0.054	0.089		
DIAG2	18700.0	737.0	88.9	0.483	8.03	0.052	0.088		
DIAG-FULL	16700.0	610.0	94.2	0.470	9.21	0.047	0.083		
DIAG-FULL-noimp	15300.0	604.0	98.6	0.483	10.0	0.056	0.090		
PROG-AP	22500.0	726.0	115.0	0.366	6.11	0.055	0.099	5.65	0.457
PROG-AP-noimp	10500.0	605.0	179.0	0.375	11.2	0.069	0.116	10.5	0.683

Table 6. Annual mean deposition of sulfate (Tg S yr^{-1}) due to the processes of in-cloud nucleation and impaction scavenging for warm (T>273.15 K), mixed (238.15<T≤273.15 K), and ice (T≤238.15 K) phase stratiform clouds, combined nucleation and impaction scavenging for warm, mixed, and ice convective clouds, total in-cloud scavenging (ICS), below-cloud scavenging (BCS), dry deposition, and sedimentation.

Sulfate	CTL	F100	F100-INT	DIAG1	DIAG2	DIAG-FULL	PROG-AP
Stratiform clouds							
Warm nucleation	23.7*	24.6*	24.7*	23.6	24.6	24.4	18.9*
Mixed nucleation	13.8*	14.1*	14.2*	10.9	12.2	12.1	8.21*
Ice nucleation	0.171*	0.388*	0.388*	0.544	0.420	0.444	0.624*
Warm impaction				0.256	0.119	0.265	
Mixed impaction				0.364	0.255	0.392	
Ice impaction				0.093	0.079	0.005	
Convective clouds							
Warm	9.33	9.02	9.02	9.33	9.11	9.06	8.26
Mixed	12.4	12.0	12.0	12.9	12.3	12.4	11.2
Ice	0.72	0.70	0.70	0.78	0.73	0.77	0.70
Total ICS	60.1	60.8	61.0	58.8	59.8	59.9	48.0
Total BCS	9.67	8.96	8.91	10.9	9.97	9.91	14.9
Dry deposition	2.02	2.00	1.98	1.94	1.91	1.89	3.72
Sedimentation	1.22	1.32	1.24	1.10	1.06	1.04	6.11

* indicates that stratiform nucleation and impaction are included together in the result shown for stratiform nucleation.

Table 7. Similar to Table 6 except for black carbon deposition (Tg yr^{-1}).

Black carbon	CTL	F100	F100-INT	DIAG1	DIAG2	DIAG-FULL	PROG-AP
Stratiform clouds							
Warm nucleation	1.86*	2.10*	1.86*	1.49	1.61	1.75	1.39*
Mixed nucleation	1.16*	1.14*	1.17*	0.635	0.766	0.861	0.582*
Ice nucleation	0.014*	0.017*	0.031*	0.055	0.039	0.052	0.073*
Warm impaction				0.439	0.413	0.088	
Mixed impaction				0.217	0.197	0.081	
Ice impaction				0.012	0.009	0.001	
Convective clouds							
Warm	1.04	1.00	1.03	1.06	1.03	1.04	0.972
Mixed	1.86	1.79	1.87	1.92	1.85	1.94	1.77
Ice	0.121	0.116	0.122	0.126	0.121	0.132	0.121
Total ICS	6.06	6.17	6.08	5.95	6.03	5.94	4.96
Total BCS	0.980	0.886	0.955	1.09	1.02	1.09	1.53
Dry deposition	0.706	0.684	0.711	0.687	0.687	0.701	0.828
Sedimentation	0.024	0.023	0.024	0.024	0.024	0.024	0.436

* indicates that stratiform nucleation and impaction are included together in the result shown for stratiform nucleation.

ACPD
9, 22041–22101, 2009

Table 8. Similar to Table 6 except for particulate organic matter (POM) deposition (Tg yr^{-1}).

Organic matter	CTL	F100	F100-INT	DIAG1	DIAG2	DIAG-FULL	PROG-AP
Stratiform clouds							
Warm nucleation	14.9*	16.3*	15.3*	12.9	14.0	14.3	9.85*
Mixed nucleation	6.36*	6.20*	6.29*	3.94	4.66	4.83	3.14*
Ice nucleation	0.082*	0.110*	0.169*	0.376	0.277	0.318	0.476*
Warm impaction				1.71	1.53	0.417	
Mixed impaction				0.698	0.606	0.299	
Ice impaction				0.066	0.045	0.004	
Convective clouds							
Warm	10.1	9.86	9.99	10.3	10.0	10.1	9.51
Mixed	20.6	20.1	20.5	21.2	20.5	21.1	19.6
Ice	1.40	1.37	1.40	1.45	1.41	1.50	1.40
Total ICS	53.4	53.9	53.7	52.6	53.0	52.9	44.2
Total BCS	6.75	6.32	6.48	7.53	7.12	7.30	11.3
Dry deposition	5.92	5.88	5.91	5.82	5.83	5.80	7.05
Sedimentation	0.194	0.186	0.187	0.200	0.199	0.203	3.71

* indicates that stratiform nucleation and impaction are included together in the result shown for stratiform nucleation.

Table 9. Similar to Table 6 except for dust deposition (Tg yr^{-1}).

Dust	CTL	F100	F100-INT	DIAG1	DIAG2	DIAG-FULL	PROG-AP
Stratiform clouds							
Warm nucleation	25.8*	31.5*	16.4*	15.4	16.8	15.2	10.2*
Mixed nucleation	29.5*	31.7*	17.7*	10.6	13.8	11.0	7.72*
Ice nucleation	0.308*	0.474*	1.04*	2.05	1.24	0.964	0.936*
Warm impaction				0.030	0.027	12.1	
Mixed impaction				0.191	0.172	13.6	
Ice impaction				0.088	0.085	0.002	
Convective clouds							
Warm	23.7	22.5	24.4	24.6	24.7	23.2	26.1
Mixed	34.4	32.9	36.0	37.1	36.9	35.1	39.3
Ice	2.31	2.18	2.37	2.41	2.45	2.45	2.69
Total ICS	116.0	121.0	97.9	92.5	96.2	114.0	87.2
Total BCS	81.8	77.4	95.2	103.0	99.7	86.8	104.0
Dry deposition	21.1	20.9	21.7	22.1	22.0	21.4	23.4
Sedimentation	122.0	120.0	124.0	126.0	126.0	123.0	129.0

* indicates that stratiform nucleation and impaction are included together in the result shown for stratiform nucleation.

Table 10. Similar to Table 6 except for sea salt ($Tg\,yr^{-1}$).

Sea salt	CTL	F100	F100-INT	DIAG1	DIAG2	DIAG-FULL	PROG-AP
Stratiform clouds							
Warm nucleation	740.0*	753.0*	753.0*	763.0	777.0	776.0	494.0*
Mixed nucleation	624.0*	701.0*	704.0*	572.0	622.0	629.0	310.0*
Ice nucleation	0.41*	1.05*	1.04*	3.06	1.50	1.54	2.64*
Warm impaction				0.044	0.019	2.64	
Mixed impaction				0.096	0.056	3.53	
Ice impaction				0.001	0.0004	0.022	
Convective clouds							
Warm	285.0	282.0	282.0	284.0	280.0	282.0	304.0
Mixed	328.0	322.0	321.0	334.0	324.0	333.0	371.0
Ice	9.65	9.49	9.49	10.0	9.67	10.2	11.9
Total ICS	1990.0	2070.0	2070.0	1970.0	2010.0	2040.0	1500.0
Total BCS	1240.0	1200.0	1200.0	1290.0	1260.0	1250.0	1530.0
Dry deposition	933.0	913.0	913.0	915.0	912.0	910.0	1020.0
Sedimentation	1250.0	1230.0	1220.0	1220.0	1220.0	1210.0	1330.0

* indicates that stratiform nucleation and impaction are included together in the result shown for stratiform nucleation.

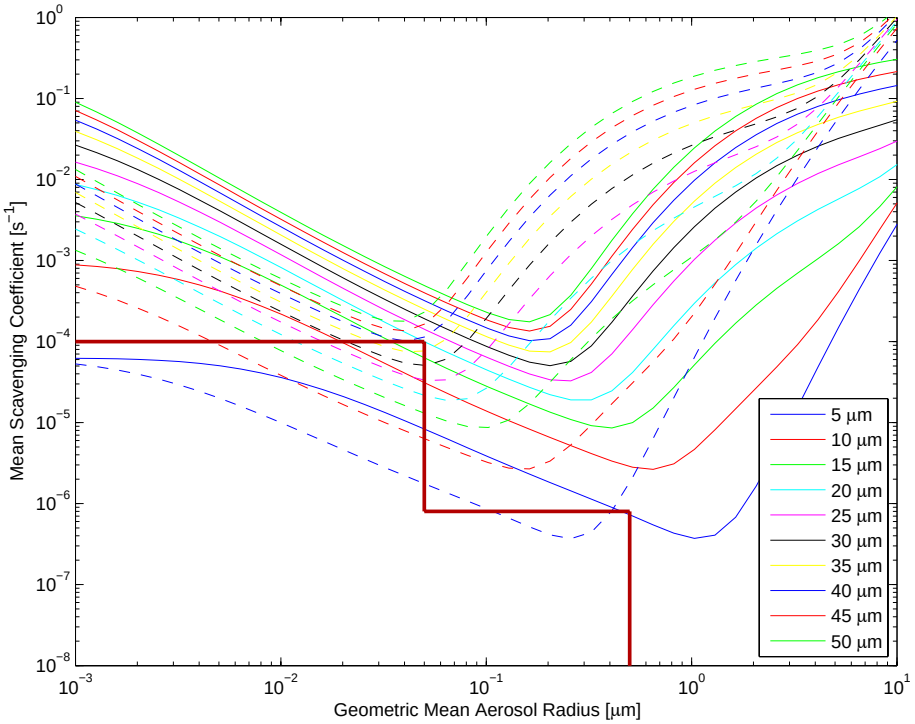

Fig. 1. In-cloud mean mass (dashed lines) and number (solid lines) impaction scavenging coefficients (s^{-1}) as a function of geometric mean aerosol radius, for a cloud droplet number concentration of 40 cm^{-3}, and for a range of mean cloud droplet sizes from 5 to 50 μm. The prescribed cloud droplet collection coefficients of Hoose et al. (2008a,b) are shown by the red steps.

ACPD
9, 22041–22101, 2009

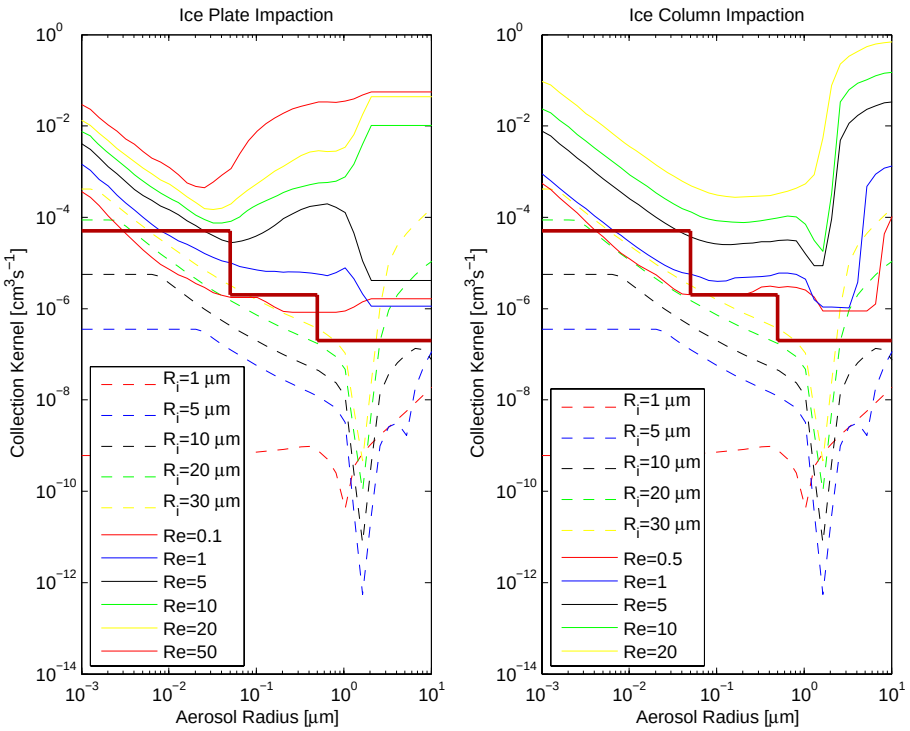

Fig. 2. Impaction scavenging kernels ($cm^3\,s^{-1}$) for in-cloud ice crystal–aerosol collisions as a function of ice crystal Reynold's number following Miller and Wang (1991) (solid lines), and for both columns and plates. The dashed lines are for droplet–aerosol collisions. The prescribed ice crystal collection kernels of Hoose et al. (2008a,b) are shown by the red steps.

ACPD
9, 22041–22101, 2009

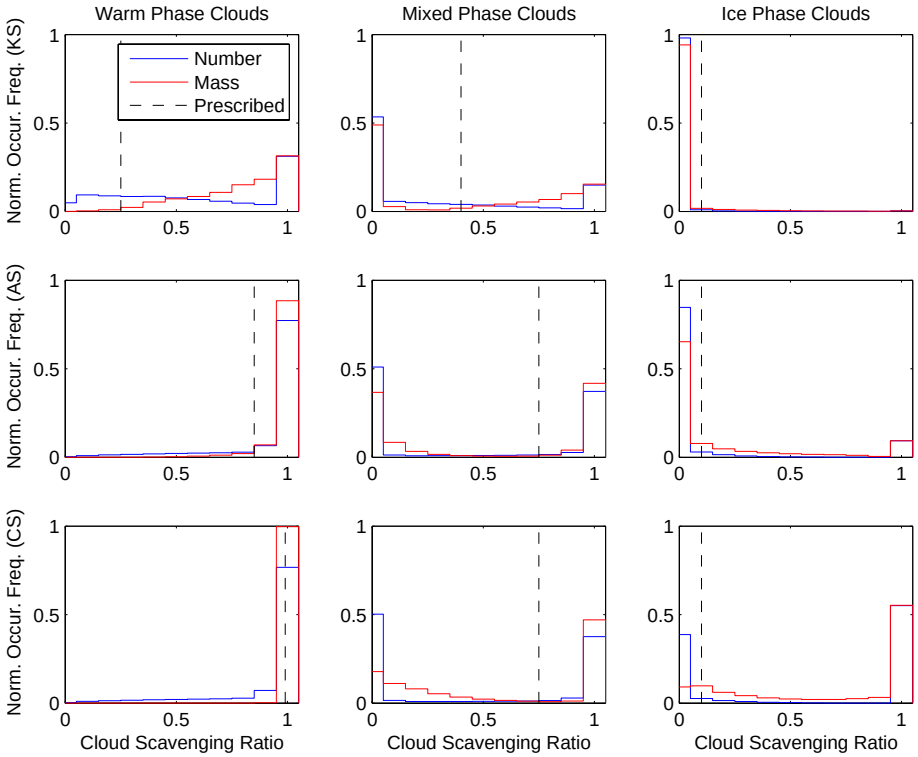

Fig. 3. Histograms of the frequency of occurrence of the stratiform in-cloud mass and number scavenging ratios for the simulation DIAG-FULL, including both nucleation and size-dependent impaction scavenging for the internally mixed/soluble Aitken (KS), accumulation (AS), and coarse (CS) aerosols modes, and for warm (T>273.15 K), mixed (238.15<T≤273.15 K) and ice (T≤238.15 K) phase clouds. The dashed line indicates the prescribed ratios of Stier et al. (2005) used for the CTL simulation.

ACPD
9, 22041–22101, 2009

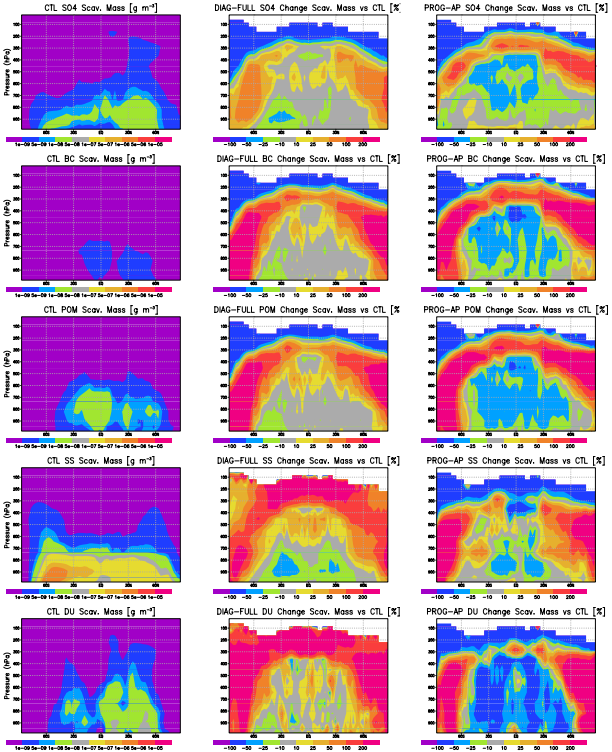

Fig. 4. Zonal and annual mean sulfate (SO_4), black carbon (BC), particulate organic matter (POM), sea salt (SS), and dust (DU) mass (g m^{-3}, except g S m^{-3} for sulfate) contained in cloud droplets and ice crystals for the simulation CTL and the percent change in these scavenged masses for the simulations DIAG-FULL and PROG-AP as compared to the CTL simulation.

ACPD
9, 22041–22101, 2009

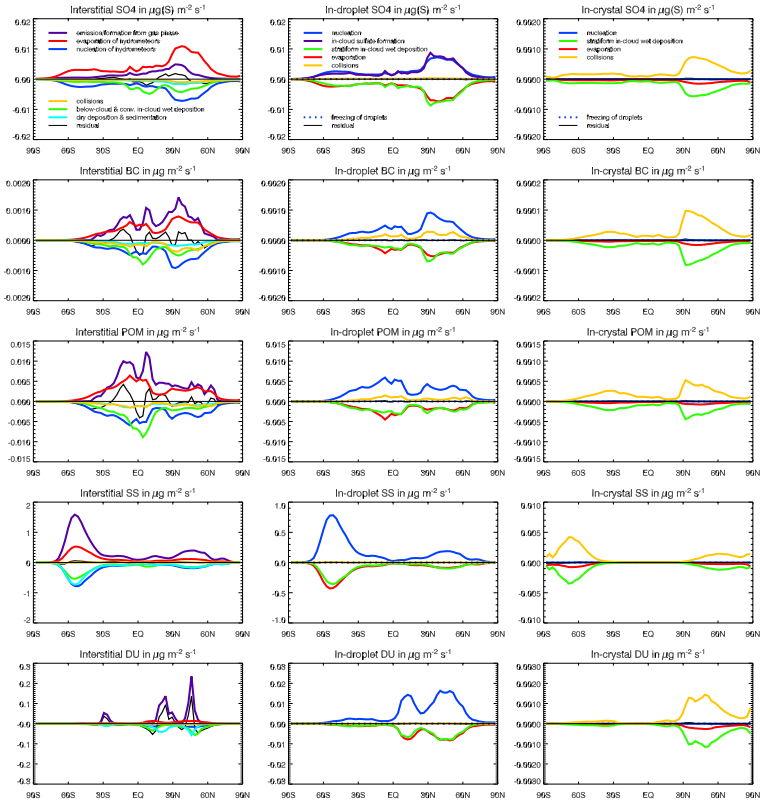

Fig. 5. The zonal and annual mean transfer rates ($\mu g\,m^{-2}\,s^{-1}$, except $\mu g\,S\,m^{-2}\,s^{-1}$ for sulfate) between the interstitial, in-droplet and in-crystal aerosol modes for the simulation PROG-AP due to the processes of emission/formation from gas phase, droplet and ice crystal nucleation, droplet freezing, aerosol collisions with droplets and ice crystals, below-cloud and in-cloud wet deposition, dry deposition, and sedimentation.

ACPD
9, 22041–22101, 2009

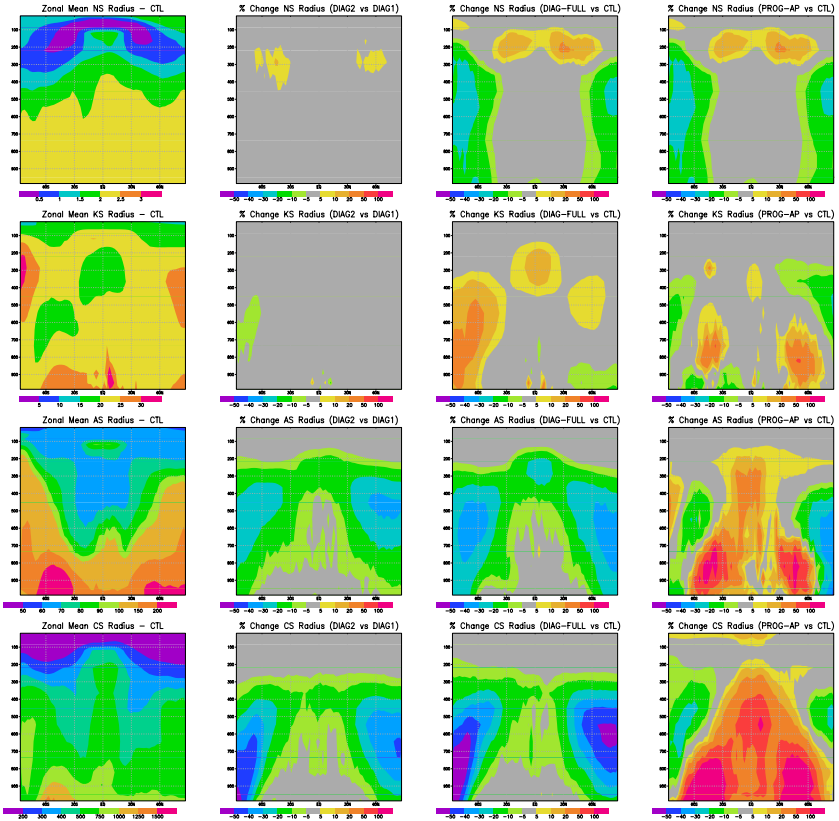

Fig. 6. Zonal and annual mean count median aerosol radius (nm) for the CTL simulation for the four soluble/internally mixed modes, nucleation (NS), Aitken (KS), accumulation (AS), and coarse (CS), and the percent change of the zonal and annual mean count median aerosol radius for the simulation DIAG2 relative to the simulation DIAG1, and for DIAG-FULL and PROG-AP simulations relative to the CTL simulation.

ACPD
9, 22041–22101, 2009

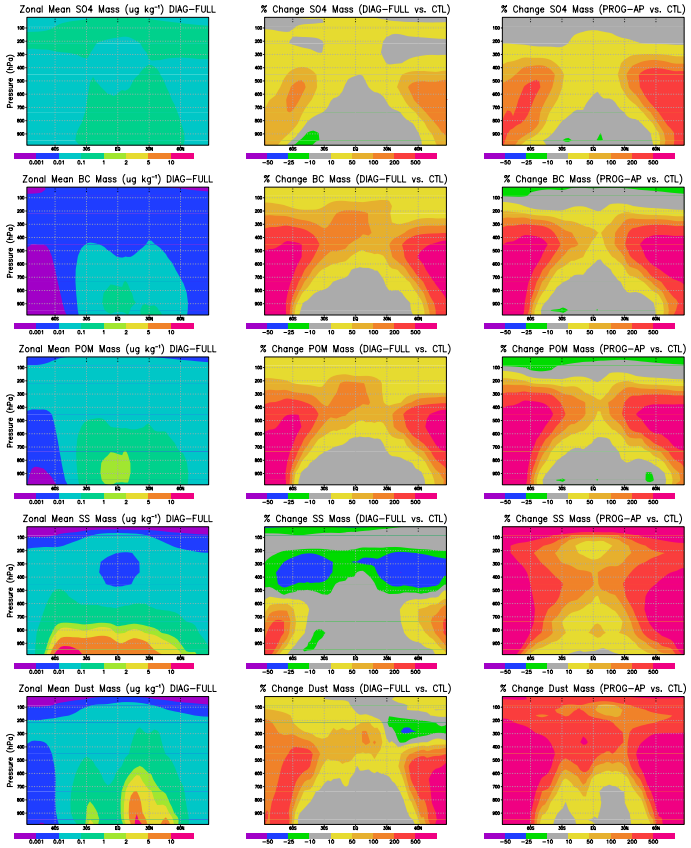

Fig. 7. The zonal and annual mean sulfate (SO_4), black carbon (BC), particulate organic matter (POM), sea salt (SS), and dust (DU) mass mixing ratios ($\mu g\,kg^{-1}$, except $\mu g\,S\,kg^{-1}$ for sulfate) for the simulation DIAG-FULL and the percent change in these masses for the simulations DIAG-FULL and PROG-AP as compared to the simulation CTL.

ACPD
9, 22041–22101, 2009

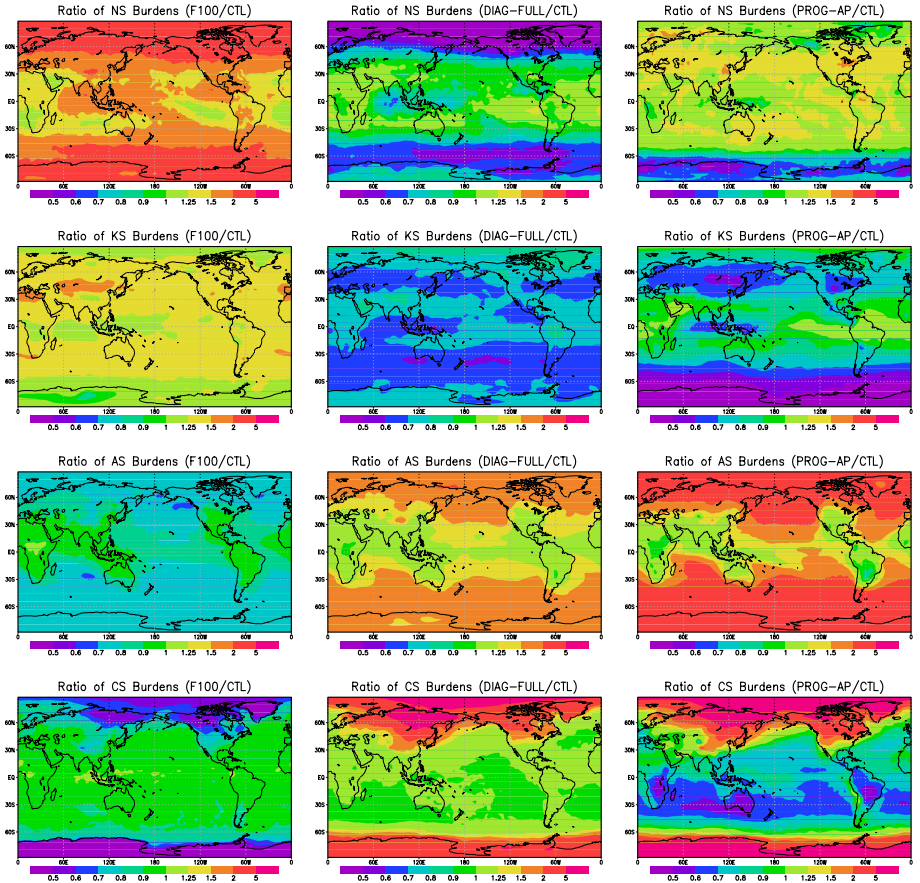

Fig. 8. The geographic distribution of the ratio of the vertically integrated number burdens for the four soluble/internally mixed modes (nucleation (NS), Aitken (KS), accumulation (AS), and coarse (CS)) for the simulations F100, DIAG-FULL, and PROG-AP as compared to the CTL simulation. For the PROG-AP simulation, these are interstitial mode number burdens only.

ACPD
9, 22041–22101, 2009

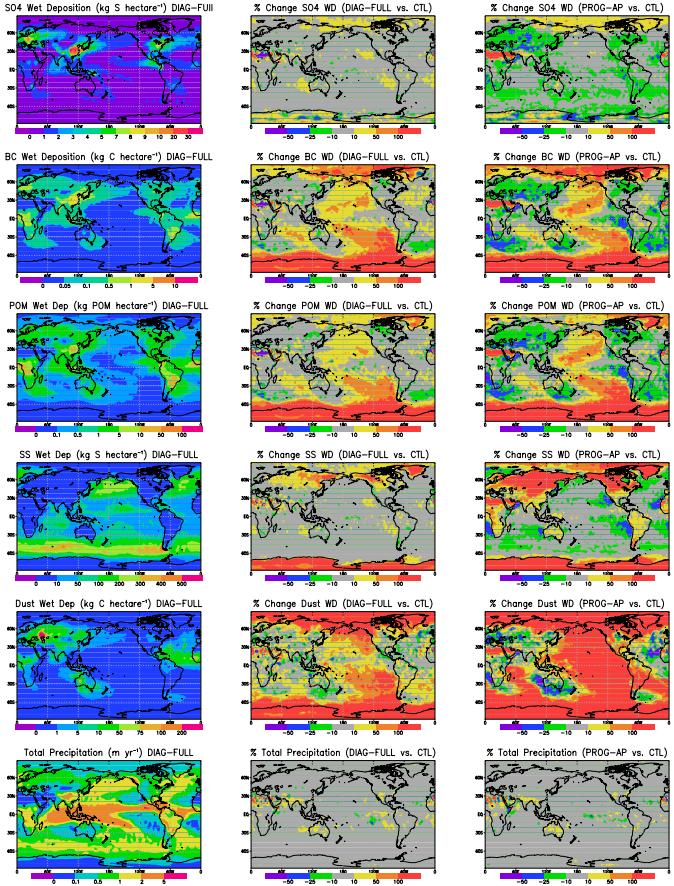

Fig. 9. The geographic distribution of sulfate (SO_4), black carbon (BC), particulate organic matter (POM), sea salt (SS) and dust annual mean wet deposition (kg ha^{-1} yr^{-1}, except kg S ha^{-1} yr^{-1} for sulfate), and total precipitation for the DIAG-FULL simulation, and the percent change for the simulations DIAG-FULL and PROG-AP as compared to the CTL simulation.

ACPD
9, 22041–22101, 2009

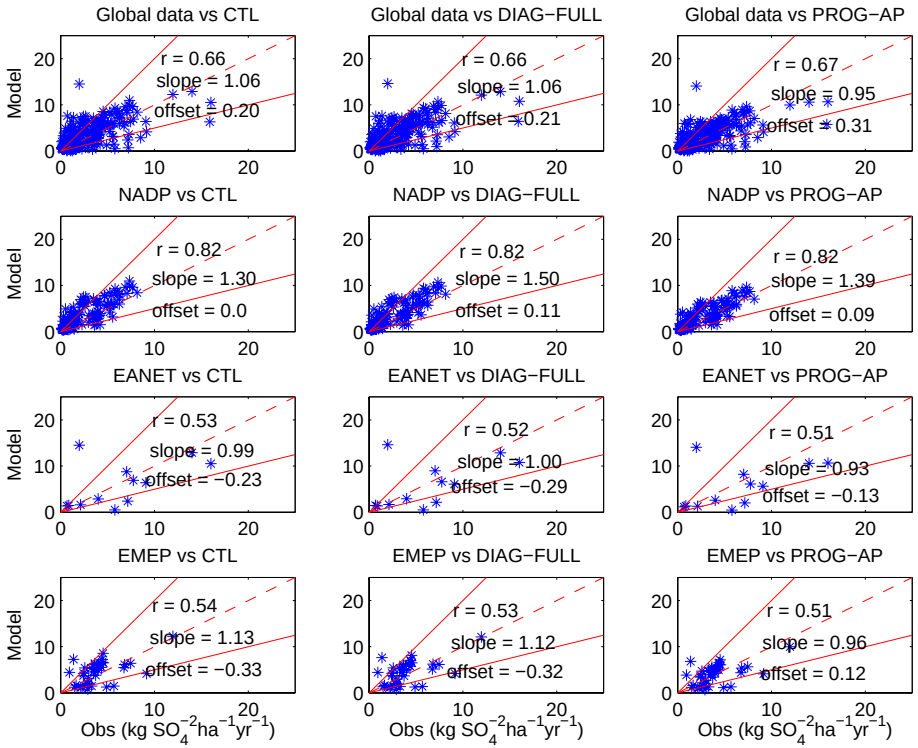

Fig. 10. The annual mean sulfate wet deposition (kg SO_4^{-2} ha^{-1} yr^{-1}) grouped by global region from observations (Dentener et al., 2006a) as compared to the simulations CTL, DIAG-FULL and PROG-AP.

ACPD
9, 22041–22101, 2009

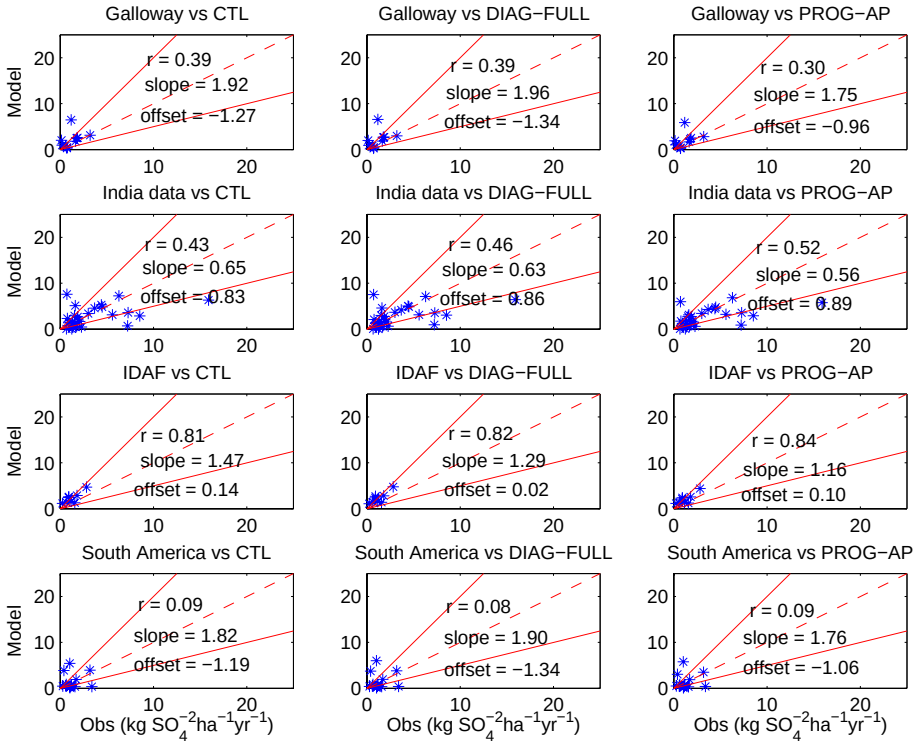

Fig. 11. The annual mean sulfate wet deposition (kg SO_4^{-2} ha^{-1} yr^{-1}) grouped by global region from observations (Dentener et al., 2006a) as compared to the simulations CTL, DIAG-FULL and PROG-AP.

ACPD
9, 22041–22101, 2009

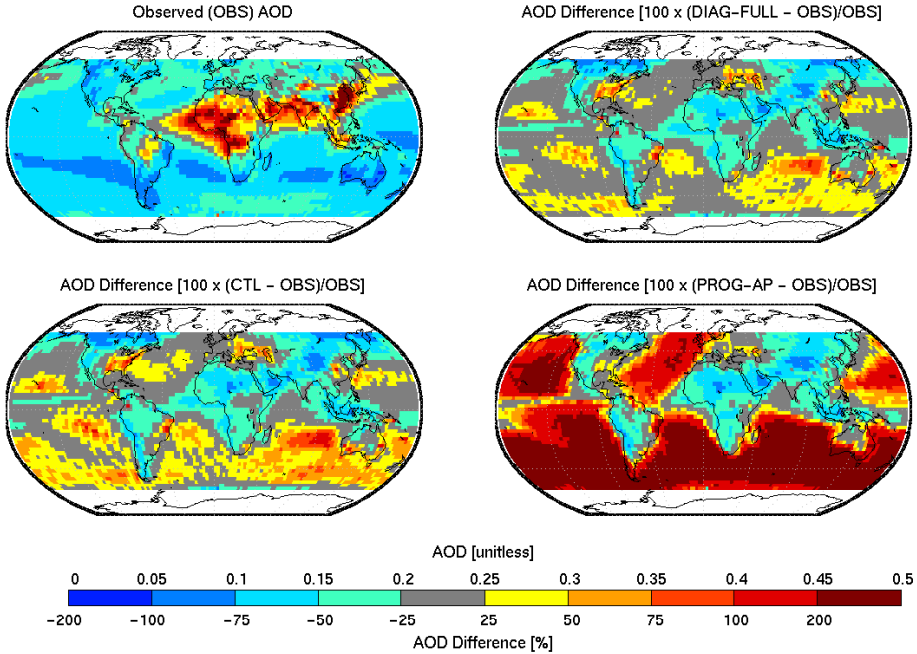

Fig. 12. The geographic distribution of annual mean aerosol optical depth (AOD) at 550 nm from the composite MODIS, MISR, AERONET dataset compiled by van Donkelaar et al. (2009) and the percent difference for the simulations CTL, DIAG-FULL, and PROG-AP as compared to the observations.

ACPD
9, 22041–22101, 2009

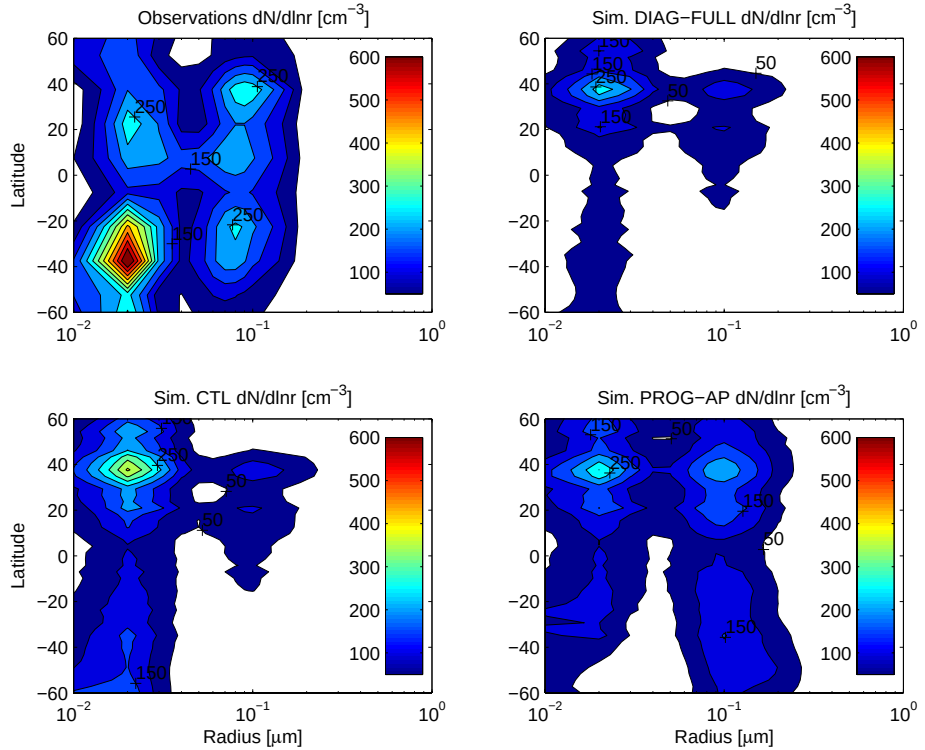

Fig. 13. Zonal mean aerosol size distributions in the marine boundary layer for the simulations CTL, DIAG-FULL, and PROG-AP as compared to the observations of Heintzenberg et al. (2000), and similar to Fig. 8 of Hoose et al. (2008a).

ACPD
9, 22041–22101, 2009

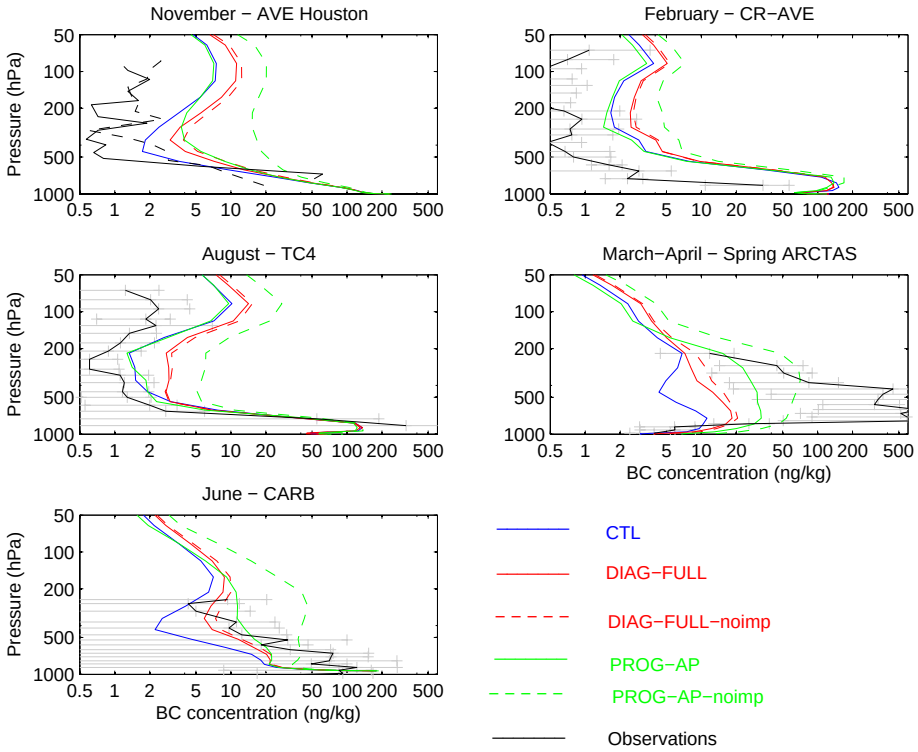

Fig. 14. Black carbon concentrations (ng kg^{-1}) from the tropical and mid-latitude aircraft campaigns over the Americas, described in detail in Koch et al. (2009), and for the simulations CTL, DIAG-FULL, and PROG-AP, and with no impaction scavenging for DIAG-FULL-noimp and PROG-AP-noimp.

ACPD
9, 22041–22101, 2009

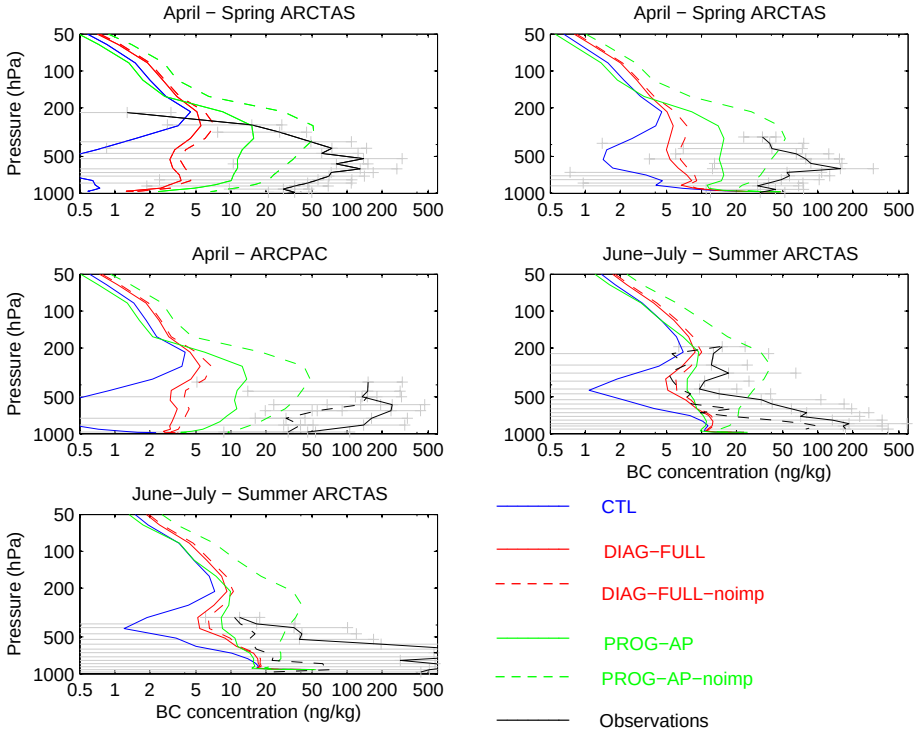

Fig. 15. Black carbon concentrations (ng kg^{-1}) from the high latitude aircraft campaigns over the Americas, described in detail in Koch et al. (2009), and for the simulations CTL, DIAG-FULL, and PROG-AP, and with no impaction scavenging for DIAG-FULL-noimp and PROG-AP-noimp.

ACPD
9, 22041–22101, 2009

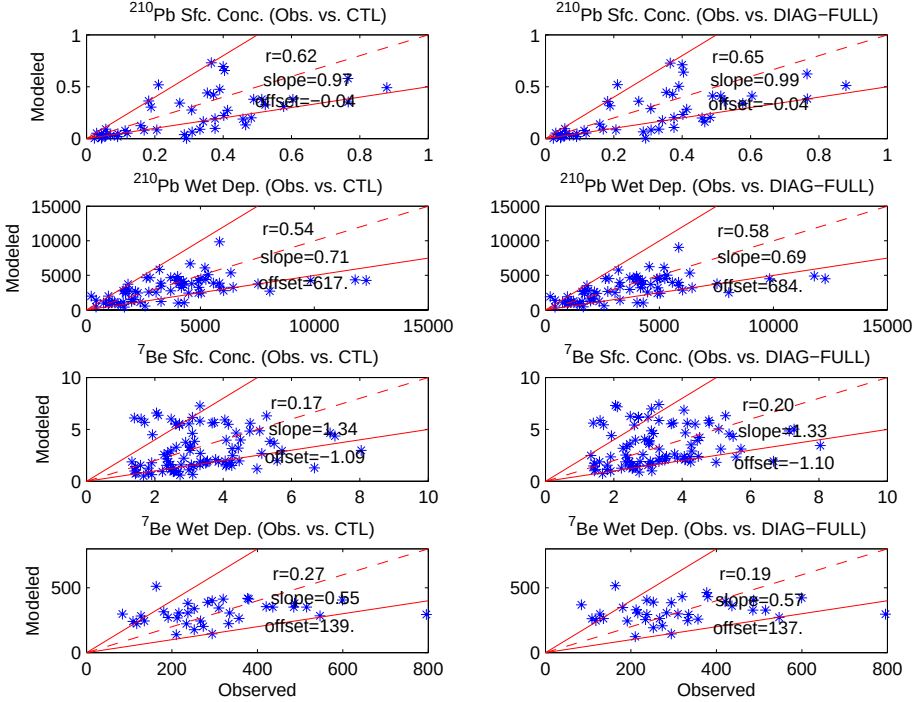

Fig. 16. Annual mean surface layer concentrations (mBq m^{-3} at STP) and wet deposition (atoms m^{-2} s^{-1}) of ^{210}Pb and ^{7}Be from observations compared to the simulations CTL and DIAG-FULL.

ACPD
9, 22041–22101, 2009